ACS Chemical Neuroscience
Cite This: ACS Chem. Neurosci. 2019, 10, 252−265
Research Article
pubs.acs.org/chemneuro

4,6-Diphenylpyrimidine Derivatives as Dual Inhibitors of Monoamine Oxidase and Acetylcholinesterase for the Treatment of Alzheimer's Disease

Bhupinder Kumar,[†] Ashish Ranjan Dwivedi,[†] Bibekananda Sarkar,[‡] Sukesh Kumar Gupta,[§] Sairam Krishnamurthy,[§] Anil K. Mantha,[‡] Jyoti Parkash,[‡] and Vinod Kumar*[,†]

[†]Laboratory of Organic and Medicinal Chemistry, Department of Pharmaceutical Sciences and Natural Products, Central University of Punjab, Bathinda, Punjab 151001, India

[‡]Department of Animal Sciences, School of Basic and Applied Sciences, Central University of Punjab, Bathinda, Punjab 151001, India

[§]Department of Pharmaceutical Engineering and Technology, Indian Institute of Technology (Banaras Hindu University), Varanasi 221005, India

Supporting Information

ABSTRACT: Alzheimer's disease (AD) is a neurodegenerative disorder with multifactorial pathogenesis. Monoamine oxidase (MAO) and acetylcholinesterase enzymes (AChE) are potential targets for the treatment of AD. A total of 15 new propargyl containing 4,6-diphenylpyrimidine derivatives were synthesized and screened for the MAO and AChE inhibition activities along with ROS production inhibition and metal-chelation potential. All the synthesized compounds were found to be selective and potent inhibitors of MAO-A and AChE enzymes at nanomolar concentrations. **VB1** was found to be the most potent MAO-A and BuChE inhibitor with IC_{50} values of 18.34 ± 0.38 nM and 0.666 ± 0.03 μM, respectively. It also showed potent AChE inhibition with an IC_{50} value of 30.46 ± 0.23 nM. Compound **VB8** was found to be the most potent AChE inhibitor with an IC_{50} value of 9.54 ± 0.07 nM and displayed an IC_{50} value of 1010 ± 70.42 nM against the MAO-A isoform. In the cytotoxic studies, these compounds were found to be nontoxic to the human neuroblastoma SH-SY5Y cells even at 25 μM concentration. All the compounds were found to be reversible inhibitors of MAO-A and AChE enzymes. In addition, these compounds also showed good neuroprotective properties against 6-OHDA- and H_2O_2-induced neurotoxicity in SH-SY5Y cells. All the compounds accommodate nicely to the hydrophobic cavity of MAO-A and AChE enzymes. In the molecular dynamics simulation studies, both **VB1** and **VB8** were found to be stable in the respective cavities for 30 ns. Thus, 4,6-diphenylpyrimidine derivatives can act as promising leads in the development of dual-acting inhibitors targeting MAO-A and AChE enzymes for the treatment of Alzheimer's disease.

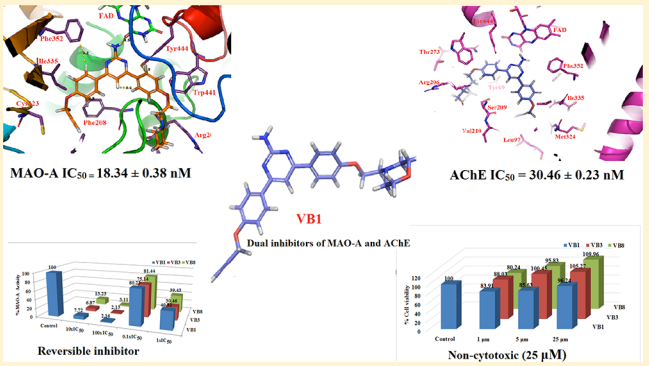

KEYWORDS: *Alzheimer's disease, MAO inhibitors, diphenylpyrimidine, acetylcholinesterase inhibitors, dual inhibitors, neuroprotective agents*

INTRODUCTION

Alzheimer's disease (AD) is a multifactorial neurodegenerative disorder characterized by the progressive memory loss, dementia, and other cognitive impairments.[1] It is estimated that 1 in every 3 senior persons dies with AD and 1 in 10 persons over 65 years of age has AD.[2] According to Alzheimer's association, in recent years' deaths due to stroke, heart disease, and HIV decreased 21%, 14%, and 54%, respectively, whereas deaths from AD increased 89%.[2] The exact molecular pathogenesis of AD is not clear; however, in most of the cases, the disease state is linked with the degeneration of neurons and glial cells or inclined metabolism of signaling neurotransmitters. Various biochemical and histopathological studies indicated that overexpressed monoamine oxidase (MAO) enzyme, low acetylcholine levels, amyloid-β (Aβ) deposits,[3] hyper-phosphorylated tau-protein aggregation, and oxidative stress play crucial roles in the pathophysiology of the disease. Depressive symptoms occur in patients suffering with AD and these may be associated with the decreased serotonergic and noradrenergic transmission in the limbic system,[4,5] Hyperactivation of MAO enzyme has been observed in patients suffering with AD that decreases the

Received: May 4, 2018
Accepted: October 8, 2018
Published: October 8, 2018

DOI: 10.1021/acschemneuro.8b00220
ACS Chem. Neurosci. 2019, 10, 252−265

Scheme 1. Reaction Scheme for the Synthesis of Target Molecules[a]

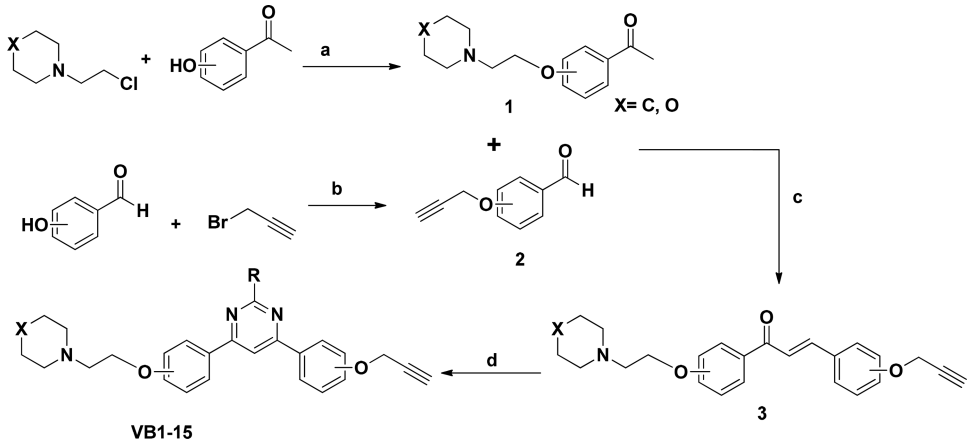

[a]Reagents and conditions: (a) K_2CO_3, KI, acetone, reflux, 6 h; (b) K_2CO_3, acetone, reflux, 6 h; (c) CH_3OH, 10% NaOH aq, rt, stirring, 3 h; and (d) Na_2CO_3, CH_3CN, amidine/guanidine/benzamidine, reflux, 24 h

concentration of dopaminergic and serotoninergic neurotransmitters. Some clinical trials have shown that deprenyl, a potential MAO-B inhibitor, alleviate the symptoms of AD.[6−8] Acetylcholine is an important neurotransmitter in the regulation of learning and memory processes. It is hydrolyzed by acetylcholinesterase (AChE) and cholinesterase inhibitors enhance the level of acetylcholine. Thus, cholinergic system has been explored as an important target for the treatment of AD. Currently, tacrine, donepezil,[9] galantamine,[10] and rivastigmine[11] are FDA (U.S. Food and Drug Administration) approved drugs that improve AD symptoms by inhibiting AChE.[11−13] Apart from the beneficial palliative properties of AChE inhibitors in AD,[14] cholinergic drugs have shown little efficacy to prevent the progression of the disease. Consequently, there is no efficient drug to cure, stop, or even slow the progression of the disease, and therefore, effective therapeutics are sought for the permanent treatment of AD.[15,16]

The pathogenesis of AD is complex, and targeting a single pathway may not be an effective strategy for the complete treatment of the disease. Multitargeted ligands design strategy involves the incorporation of two or more distinct pharmacophores of different drugs in the single structure to develop hybrid molecules.[17,18] Hence, the multitargeting ligands which can simultaneously inhibit MAO, AChE, and BuChE enzymes are being developed as drugs for the management/treatment of AD.[19,20] A number of multitargeting ligands have been reported as potential therapeutic agents for the treatment of AD.[21,22] Although many newly developed MAO, AChE, and BuChE inhibitors are under different phases of clinical trials, none of these has reached clinical use because of the number of adverse effects. Recently, we have reported various phenyl-/benzhydrylpiperazine derivatives[23] as selective ligands for MAO-A and MAO-B isoforms. In another study, we have synthesized and screened a number of pyrimidine bridged biaryls[24] for their MAO inhibition potential. Most of these compounds were found to be reversible and selective inhibitors of the MAO-B isoform. There is a high structural resemblance between the two isoforms of MAO enzyme. The volume of entrance cavity of MAO-B is smaller (~300 Å^3) as compared with the active cavity of MAO-A (~400 Å^3).[6,21] Thus, MAO-B accommodates smaller molecules, while bulkier ligands selectively bind to the MAO-A isoform. A small alteration in the structure of ligand can change its preference for either of the isoforms (MAO-A or MAO-B). Taking leads from these studies, we became interested in the design and synthesis of dual acting ligands that are equipotent to both MAO and AChE enzymes for the treatment of AD. From the literature search, we noted that the propargylamino group plays an important role in providing the neuronal and mitochondrial protective properties.[25,26] The propargyl group is also involved in the crucial covalent bond formation with FAD cofactor of MAO enzyme. Similarly, in the literature survey, it has been observed that most of the AChE inhibitors, such as donepezil, rivastigmine, pyridostigmine, phenserine galantamine, among others, contained a tertiary amino group in the scaffold as a part of ring or open chain.[9−13,27] Hence, we presumed that a tertiary nitrogen atom might be playing a crucial role for the AChE inhibition activity and introduced a piperidine/morpholine ring in the scaffold as potential pharmacophore for the AChE enzyme. The chain length between the propargyl and piperidine moieties is reported to control the dual interaction of these moieties with both the catalytic active site and peripheral anionic site of the AChE enzyme.[28] It is envisaged that incorporation of a piperidine/morpholine ring in the scaffold would make the molecules bulkier, and these compounds might show selectivity toward the MAO-A isoform.

Thus, on the basis of our previous experience and with the aim of developing dual inhibitors, a series of 4,6-diphenylpyrimidine derivatives (**VB1**-**VB15**) have been designed with a propargyl group and a piperidine/morpholine moiety as potential pharmacophores for the MAO and AChE enzymes. These compounds were found to be potent inhibitors of both MAO and AChE enzymes with IC_{50} values in nanomolar range. All the compounds were found to be reversible inhibitors of the MAO-A and AChE enzymes and displayed no toxicity to the human neuroblastoma SH-SY5Y cells. Most of these compounds were also found to be inhibitors of BuChE in the micro molar range. In the molecular dynamics simulation studies of 30 ns, the most potent MAO inhibitor (**VB1**) and most potent AChE inhibitor (**VB8**) were found quite stable in the active sites of the enzymes. These compounds also displayed neuroprotective potential against 6-OHDA and H_2O_2 induced neurotoxicity in SH-SY5Y cells.

DOI: 10.1021/acschemneuro.8b00220
ACS Chem. Neurosci. 2019, 10, 252−265

Table 1. Results of the MAO, AChE, and BuChE Inhibition Studies of Synthesized Compounds

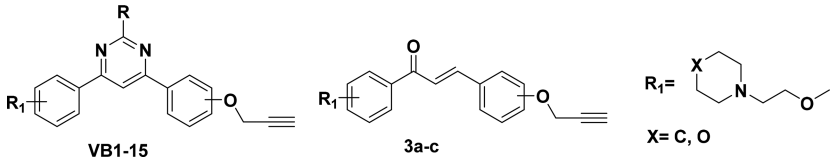

entry name	R_1	R	propargyl group position	X	IC_{50} values (mean ± SE nM) hMAO-A	hMAO-B	ee AChE	IC_{50} values (mean ± SE μM) eq BuChE	MAOSI
VB1	C4	NH_2	C4	O	18.34 ± 0.38	9910.14 ± 32.83	30.46 ± 0.23	0.666 ± 0.03	540
VB2	C4	C_6H_5	C4	O	86.35 ± 0.42	6915.62 ± 26.72	39.83 ± 0.39	14.84 ± 0.27	80
VB3	C4	CH_3	C4	O	28.33 ± 3.22	8409.53 ± 25.69	18.92 ± 0.29	14.98 ± 0.31	297
VB4	C4	C_6H_5	C4	C	103.42 ± 11.43	8376.28 ± 23.73	24.69 ± 0.76	19.72 ± 0.27	81
VB5	C4	CH_3	C4	C	752.63 ± 14.34	12140.12 ± 100.64	765.14 ± 3.51	54.46 ± 1.42	16
VB6	C4	C_6H_5	C3	O	2140.12 ± 50.43	14850.34 ± 80.62	1841.56 ± 27.67	8.216 ± 0.10	7
VB7	C4	NH_2	C3	O	230.12 ± 7.22	7313.76 ± 65.32	20.45. ± 0.17	16.65 ± 0.17	32
VB8	C4	CH_3	C3	O	1010 ± 70.42	12185.94 ± 190.86	9.54 ± 0.07	13.75 ± 0.23	12
VB9	C4	NH_2	C2	O	890.45 ± 8.32	8875.37 ± 110.52	2390.23 ± 20.72	161.6 ± 5.88	10
VB10	C4	C_6H_5	C2	O	690.34 ± 20.32	12305.63 ± 87.72	30105.12 ± 70.14	22.68 ± 0.36	18
VB11	C3	C_6H_5	C4	O	2430.23 ± 45.33	8974.73 ± 93.73	2269.82 ± 32.01	14.66 ± 0.20	4
VB12	C3	NH_2	C4	O	360.33 ± 2.34	8738.97 ± 51.73	1438.54 ± 27.67	23.48 ± 0.18	24
VB13	C3	CH_3	C4	O	450.44 ± 5.13	8469.63 ± 83.72	717.88 ± 7.54	15.27 ± 0.11	19
VB14	C4	C_6H_5	C3	C	1320.22 ± 30.22	9565.83 ± 120.53	2093.71 ± 15.69	15.95 ± 0.12	7
VB15	C4	NH_2	C3	C	1040.12 ± 40.12	7706.23 ± 95.73	1441.42 ± 20.33	34.79 ± 0.27	7
3a	C4	----	C4	O	260.12 ± 13.12	9320.12 ± 24.22	20427.18 ± 22.15	----	36
3b	C4	----	C2	O	313.23 ± 17.22	8110.11 ± 40.11	[a]	----	26
3c	C3	----	C4	O	532.42 ± 19.23	7809.02 ± 35.13	[a]	----	15
		clorgyline			4.39 ± 1.02	----	----	----	MAO-A
		pargyline			----	0.15 ± 0.02	----	----	MAO-B
		donepezil			----	----	11.32 ± 0.001	1.28 ± 0.04	----

[a]Inactive or showed less than 50% inhibitory activity at 50 μM concentration and precipitated at higher concentrations. IC_{50} values of BuChE are expressed in μM. MAO SI = IC_{50} of MAO-B/IC_{50} of MAO-A.

RESULTS AND DISCUSSION

Chemistry. All the compounds were synthesized as per the reaction procedures described in Scheme-1. Briefly, *O*-alkylated acetophenones (**1**) and benzaldehydes (**2**) were synthesized from corresponding hydroxy acetophenones or benzaldehydes by refluxing these with suitable alkyl halides in the presence of potassium carbonate and acetone as solvent. *O*-Alkylated acetophenones (**1**) and benzaldehydes (**2**) were reacted through aldol condensation to get the intermediate chalcones (**3**). In the final step, chalcones (**3**) were reacted with various amidines in the presence of sodium carbonate to obtain the target compounds 4,6-diphenylpyrimidine derivatives (**VB1-VB15**). All the final products were characterized by IR, ^{1}H NMR, ^{13}C NMR, ESI-MS, and HRMS.

MAO, AChE, and BuChE Enzyme Inhibition Studies. MAO inhibition potential of the synthesized 4,6-diphenylpyrimidine derivatives (**VB1−VB15**) was evaluated throughfluorimetric method using recombinant human MAO-A and MAO-B enzymes and Amplex Red assay kit.[29]Similarly, acetylcholinesterase inhibition activity was determined using Amplex Red Acetylcholine/Acetylcholinesterase assay kit (A12217) purchased from the Molecular Probes, Inc. /Invitrogen. The results of MAO inhibition studies are described in Table 1 in terms of IC_{50} values expressed in nanomolar concentrations. Morpholine or piperidine ethyl chains (R_1) were used as meta or para substituents at one of the phenyl rings. To develop structure activity relationship profile of 4,6-diphenylpyrimidines, three amidines were used with R as $-NH_2$, $-CH_3$ or $-C_6H_5$. Similarly, a second phenyl ring was substituted with a propargyl group at ortho/meta/para positions. MAO-A, MAO-B, and AChE inhibitory activities of some of the intermediate chalcones were also evaluated to compare them with the final products. Clorgyline, pargyline, and donepezil were used as standard inhibitors for MAO-A, MAO-B, and AChE enzymes, respectively. All the compounds were found to be selective toward the MAO-A isoform with IC_{50} values varying from 18 nM to 2430 nM. MAO-B inhibition activities of these compounds were found in the range of 7313 nM to 14850 nM. These compounds were also found to be potent inhibitors of AChE with IC_{50} values in nanomolar range. However, most of the compounds displayed BuChE inhibitory activity in the micro molar range (0.66 μM to 161.6 μM). **VB1** was found to be the most potent MAO-A inhibitor with IC_{50} value of 18.34 ± 0.38 nM and selectivity index (SI) of 540 over MAO-B. **VB1** was also found to be the most potent BuChE inhibitor in the series with IC_{50} value of 0.666 ± 0.03 μM. Similarly, **VB8** was found to be the most potentAChE inhibitor with IC_{50} value of 9.54 ± 0.07 nM. **VB3** was also found potent inhibitor of both AChE and MAO-A withIC_{50} values of 18.92 ± 0.29 nM and 28.33 ± 3.22 nM, respectively. All the chalcone intermediates were found less active as compared to the corresponding final products.

Reversibility Inhibition Studies. First generation MAO inhibitors were irreversible in nature and associated with severe side effects. Reversibility of the target compound is frequently

DOI: 10.1021/acschemneuro.8b00220
ACS Chem. Neurosci. 2019, 10, 252−265

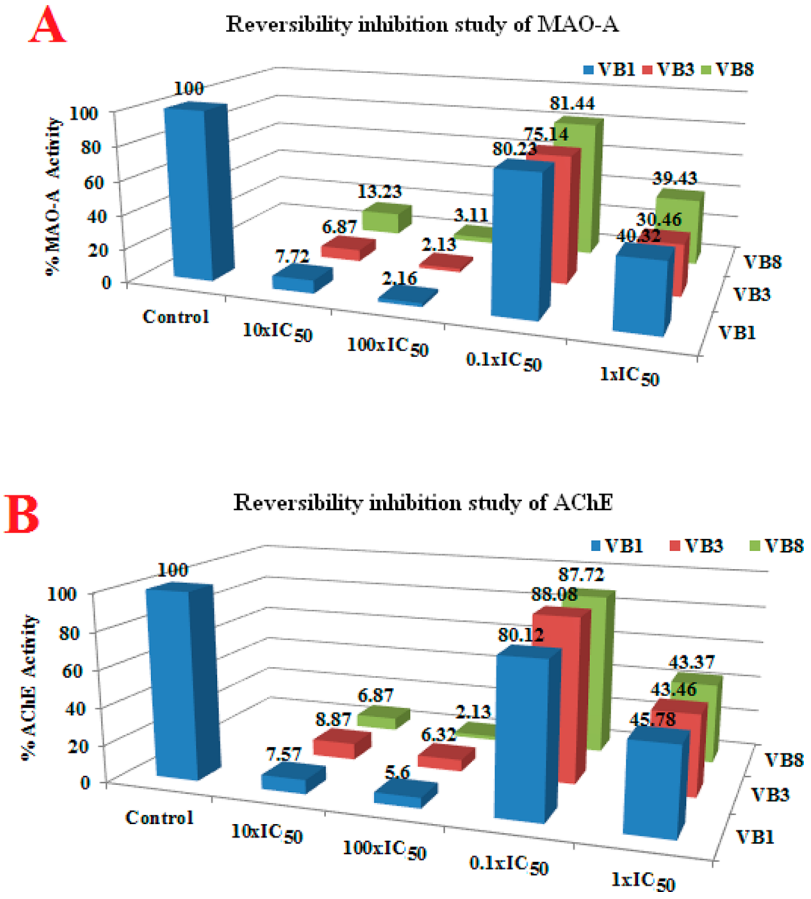

Figure 1. (A) Reversibility inhibition studies of the most potent and selective inhibitors with MAO-A enzyme; (B) Reversibility inhibition studies with AChE enzyme.

considered in designing and development of new class of inhibitors. Thus, to determine the reversible inhibition of the enzyme by the most active and selective compounds (i.e., **VB1**, **VB3** and **VB8**), reversibility inhibition studies were performed using earlier reported protocol by us and others.[23,30,31] All the tested compounds were found to be reversible inhibitors of both MAO-A and AChE enzymes. Upon treatment of MAO-A and AChE with the test compounds at concentrations of 10× IC_{50} and 100× IC_{50} activity was reduced to minimum. Upon 100 times dilution with the substrate solution, recovery of more than 75% enzymatic activity was achieved as shown in Figure 1A and Figure 1B for MAO-A and AChE respectively. Thus, it can be concluded that the tested compounds were found to be reversible inhibitors of MAO-A and AChE.

Intracellular ROS Determination. It is a well-known fact that monoamine-oxidase-mediated oxidative metabolism of monoamines leads to the production of H_2O_2 as a byproduct.[32,33] Subsequently, H_2O_2 is converted to the free radicals ($^{\bullet}OH$, $^{\bullet}O_2$) through Fenton's reaction, which contribute to the oxidative stress. An uncontrolled increase in the concentrations of the free radicals initiates free-radical-mediated chain reactions that causes oxidative damage to the cell membranes, lipid peroxidation, and DNA strand breakdown. Thus, prevention of ROS generation along with the MAO inhibition is an important strategy to reduce or eliminate neurotoxicity in neurodegenerative disorders.

Intracellular ROS level of SH-SY5Y cells was determined using nonfluorescent compound 2,7-dichlorofluorescein diacetate (DCF-DA). It is permeable and oxidized by ROS to a fluorescent compound 2,7-DCF. **VB1** was found to be the most potent ROS inhibitor and reduced the intracellular ROS level to 35.36% and 14.39% at 1 and 25 μM concentration, respectively (Figure 2). **VB3** and **VB8** also reduced the ROS levels to 42.25% and 65.25%, respectively, at 25 μM concentrations.

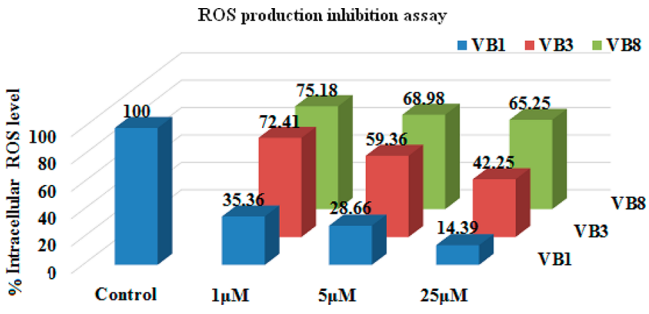

Figure 2. ROS production inhibition studies of **VB1**, **VB2**, and **VB3** against SH-SY5Y cells.

Neuroprotection Studies. The most potent compounds (**VB1**, **VB3**, and **VB8**) were evaluated for their neuroprotective potential against 6-hydroxydopamine (6-OHD) neurotoxin in the SH-SY5Y cells. However, none of the tested compounds showed promising neuroprotective potential at low concentrations (Figure 3). **VB8** was found to be the most potent among the tested compounds and displayed recovery of cells up to 61.77% at 25 μM concentration as compared with the 6-

DOI: 10.1021/acschemneuro.8b00220
ACS Chem. Neurosci. 2019, 10, 252−265

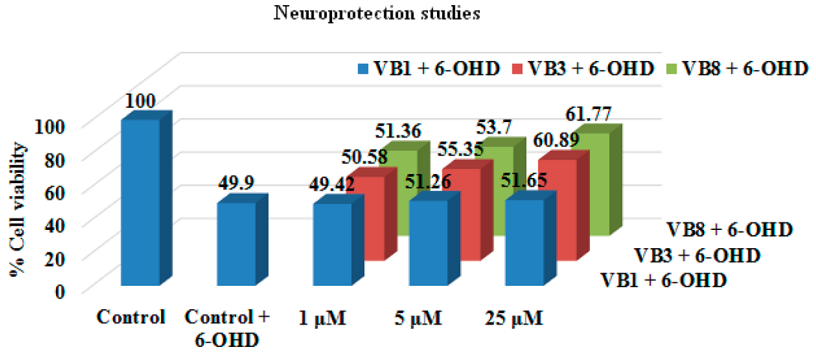

Figure 3. Neuroprotection studies of the most potent and selective MAO-A and AChE inhibitors.

OHD, which reduced the cell viability to less than 50% at 12.5 μM.

Cytotoxicity Studies. The cytotoxic effects of the most active compounds (**VB1**, **VB3**, and **VB8**) were evaluated against human neuroblastoma (SH-SY5Y) cells because of their similarity to the dopaminergic neurons.[34] The test compounds were incubated at 1, 5, and 25 μM concentrations and were analyzed after 24 h treatment time. The percentage cell viability was measured using MTT assay. As depicted in Figure 4, the compounds were found to be nontoxic against

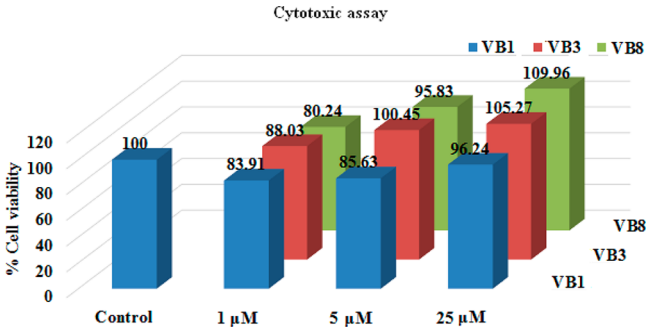

Figure 4. Cytotoxicity studies of **VB1**, **VB3**, and **VB8** against SH-SY5Y cell lines at 1, 5, and 25 μM.

the tested cells even at 25 μM concentrations. It has been observed that as concentration of the compounds increases, the percentage cell viability also increases. The least cell viability of 80% was observed with **VB8** at 1 μM concentration. Thus, keeping in view the nanomolar IC_{50} values obtained for enzyme inhibition, the current series of compounds were found to be nontoxic to the tissue cells.

Metal-Chelating Studies. Metal-chelating studies of the most potent compounds (i.e., **VB1**, **VB3**, and **VB8**) were performed with a UV−vis spectrophotometer. The absorption spectra of each compound (50 μM, final concentration) alone or in the presence of $CuSO_4$, $FeSO_4$, and $FeCl_3$ (50 μM, final concentration) was recorded. In metal-chelating studies, compounds were found to be ineffective against metals and do not form any chelates with the metal salts.

Kinetic Studies of AChE Inhibition. To determine the mechanism of inhibition of AChE, kinetic study was carried out with the most potent inhibitor of AChE (i.e., **VB8**) using eeAChE. The reciprocal Lineweaver−Burk plots (Figure 5) illustrate increased slope (decreased V_{max}) and higher intercepts (K_m) with the increasing concentration of **VB8.** The intersection point of the Lineweaver−Burk reciprocal plots was located in the second quadrant, which indicate that the inhibition mode of VB8 was mixed-type inhibition. Thus, it can be concluded that VB8 binds to both CAS and PAS of AChE simultaneously.

Molecular Docking Studies. The most potent compounds (**VB1**, **VB3**, and **VB8**) were subjected to molecular docking studies to find the interaction pattern of the molecules with the amino acid lining and their orientation at the active

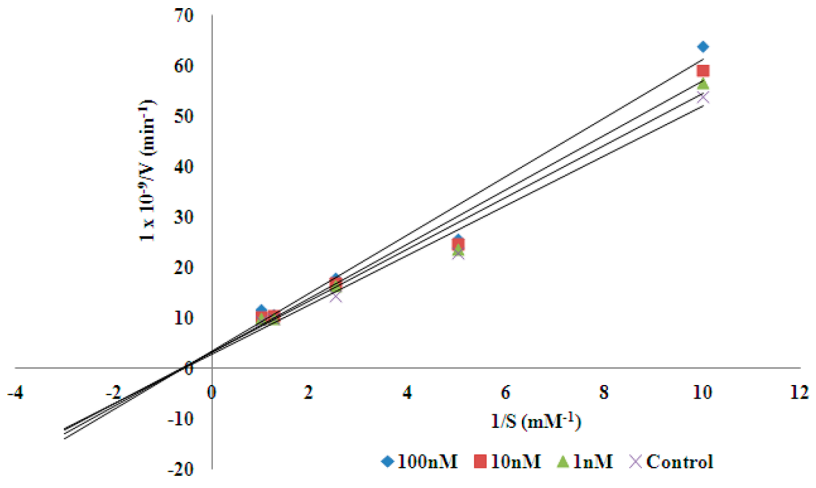

Figure 5. Kinetic study on the mechanism of ee AChE inhibition by **VB8**. Overlaid Lineweaver−Burk reciprocal plots of AChE initial velocity at increasing substrate concentration (0.1−1 mM) in the absence or presence of **VB8** are shown.

DOI: 10.1021/acschemneuro.8b00220
ACS Chem. Neurosci. 2019, 10, 252−265

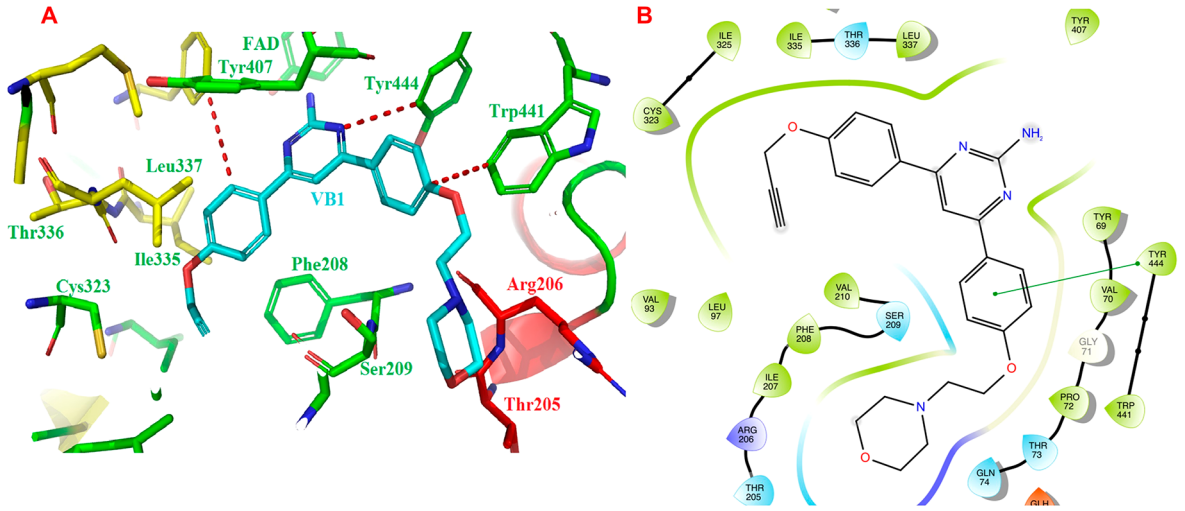

Figure 6. (A) Binding pattern (3D) of **VB1** with the amino acid residues at the active site of MAO-A (2BXR) and (B) binding interactions (2D) of **VB1** with various amino acids of MAO-A active cavity.

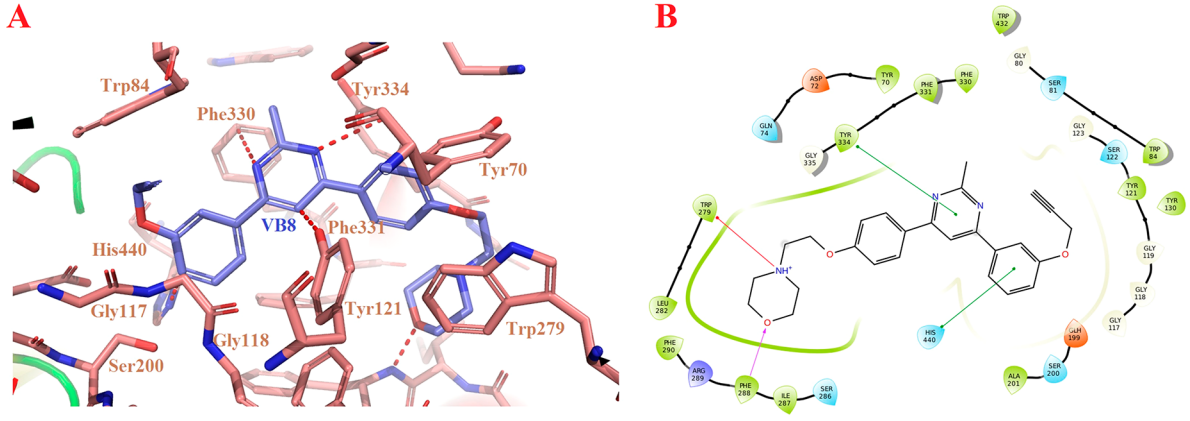

Figure 7. (A) Binding pattern (3D) of **VB8** with the amino acid residues at the active site of AChE (PDB ID 1EVE) and (B) binding interactions (2D) of **VB8** with various amino acids of AChE active cavity.

site of the receptors. Compounds were docked at the active site of hMAO-A (PDB IDs 2BXR and 2Z5X)[35,36] and AChE (PDB ID 1EVE).[37] The X-ray crystal structures were imported from the protein data bank using Maestro 11.1 (Schrödinger LLC). The docking procedure employed was first validated by redocking the cocrystallized ligands into the MAO and AChE models and the process was found suitable for the current study. Three most potent compounds (**VB1**, **VB3**, and **VB8**) were docked at the structure of MAO-A (2BXR and 2Z5X) enzymes cocrystallized with clorgyline and harmine.

All the compounds were found to accommodate nicely to the active site of MAO-A delineated by hydrophobic residues Tyr69, Phe208, Arg296, Ile335, Leu337, Phe352, Tyr407, Trp441, Tyr444, and FAD. Most of the interactions observed were hydrophobic and $\pi-\pi$ aromatic stacking which showed hydrophobic nature of the MAO-A active site. Pyrimidine moiety was aligned toward the FAD cofactor while 4-(2-phenoxyethyl)morpholine fragment was exposed to the outer part of the active site cavity lined by the polar amino acid residues Thr205 and Arg206. The (prop-2-yn-1-yloxy)benzene fragment of **VB1** showed $\pi-\pi$ aromatic interaction with Phe352, while the pyrimidine ring showed $\pi-\pi$ aromatic interaction with Tyr444. 4-(2-Phenoxyethyl)morpholine showed $\pi-\pi$ aromatic interaction with Trp441. **VB3** and **VB8** also showed interactions with the same set of amino acids at the active cavity of the enzyme (Figure S1). The only difference observed in the conformation of **VB8** was the orientation of propargyl group. In both **VB1** and **VB3**, the propargyl group was oriented toward the rest of the molecule to the inner side of the cavity, whereas in **VB8**, it was directed away from the rest of the molecule toward outer side of the cavity (Figure 6 and Figure S1). This difference in the conformation of **VB8** might be responsible for its lower activity toward MAO-A (Figures 6 and S1). The propargylamino group of clorgyline is reported to interact with FAD cofactor and form a strong covalent bond. These strong interactions might be responsible for the irreversible nature of clorgyline. As evident from Figure 6 and Figure S1, in **VB1**, **VB3** and **VB8** pyrimidine ring is aligned close to the FAD, whereas the propargyl group is oriented away from the FAD cofactor. These conformations of the ligands at the active site negate any possibility of covalent bond formation between the propargyl group and FAD. Thus, these ligands may not form strong covalent bond with the enzyme and hence display reversible inhibition activity. Son et al.[36] reported a very high-resolution structure of human MAO-A cocrystallized with a reversible MAO-A inhibitor harmine which was different from the structure reported by Colibus et al.[35] On the advice of one

DOI: 10.1021/acschemneuro.8b00220
ACS Chem. Neurosci. 2019, 10, 252−265

reviewer of this manuscript, we have also performed docking studies of reversible MAO-A inhibitor VB1 with PDB-2Z5X (Figure S2). In this case too, it has been observed that the pyrimidine ring was aligned toward the FAD cofactor, and the propargyl group was directed toward the outer part of the cavity aligned with amino acid resides Val484 and Thr487 (Figure S2). These observations further strengthen our claim that the propargyl group may not be able to form a strong covalent bond with the FAD and hence current series of compounds behave as reversible inhibitors.

Similarly, the most potent compounds (**VB1**, **VB3**, and **VB8**) were docked in the crystal structure of AChE (PDB ID 1EVE) enzyme cocrystallized with donepezil (Figures 7 and S3). All the compounds were accommodating nicely to the active site as well as the peripheral anionic site (PAS) of AChE as done by the standard inhibitor donepezil. The AChE anionic site, composed of Trp84, Tyr130, Phe330, and Phe331 residues, whereas the peripheral anionic site (PAS) consists of five amino acids-Tyr70, Asp72, Tyr121, Trp279, and Tyr334. The increased chain length between the phenyl and morpholine ring, as compared with the N-benzylpiperidine moiety of donepezil, pushed the 4-(2-phenoxyethyl)morpholine fragment of **VB1** and **VB3** inside the CAS of AChE. The morpholine moiety was aligned toward the narrowest part of the active site cavity. However, for **VB8**, the binding alignment was inverted and 4-(2-phenoxyethyl)morpholine fragment was aligned toward the 2,3-dihydroinden-1-one fragment of the donepezil (Figure 8). Thus, the (prop-2-yn-1-yloxy)benzene fragment of **VB8** was oriented toward CAS of AChE.

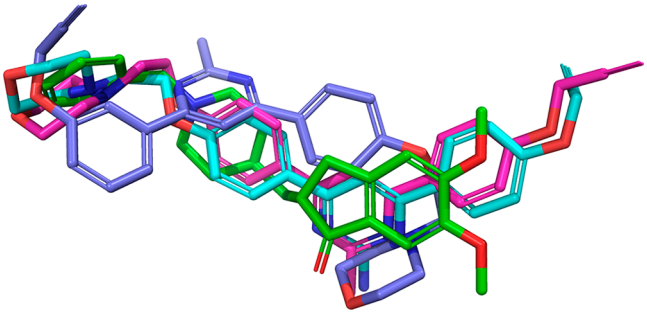

Figure 8. Superimposed poses of **VB1** (cyan), **VB3** (pink), and **VB8** (violet) with donepezil (green) at the active site of AChE (1EVE).

Comparison of the binding patterns (predicted) of donepezil and **VB8** reveals the plausible reason of its high potency for AChE. Donepezil showed $\pi-\pi$ aromatic interactions of N-benzylpiperidine fragment with Trp84 residue and cation$-\pi$ interactions with Phe331 and Tyr334 residues. The 2,3-dihydroinden-1-one fragment of the donepezil showed $\pi-\pi$ stacking with Trp279. **VB1** and **VB3** preserved most of the interactions of the donepezil with the same set of amino acid residues. These compounds showed cation$-\pi$ interactions with Trp84 and $\pi-\pi$ stacking with Trp279, Phe331, and Tyr334 residues. Similarly, pyrimidine fragment of **VB8** showed $\pi-\pi$ aromatic stacking with Phe331 and Tyr334. However, 4-(2-phenoxyethyl)morpholine fragment was aligned in the opposite direction as compared with the benzylpiperidine moiety of donepezil and displayed cation$-\pi$ interactions with the Trp279 residue and hydrogen bonding interactions with the Phe288 residue through oxygen atom of the morpholine ring (Figures 7 and S3). Furthermore, the (prop-2-yn-1-yloxy)benzene fragment of **VB8** showed additional aromatic $\pi-\pi$ stacking with His440 residue, which is not observed for **VB1**, **VB3**, and donepezil.

VB1, **VB3**, and **VB8** were superimposed with donepezil at the active site of AChE (Figure 8). The (prop-2-yn-1-yloxy)benzene fragments of **VB1** and **VB3** were oriented toward 2,3-dihydroinden-1-one fragment of the donepezil in PAS of AChE, whereas the 4-(2-phenoxyethyl)morpholine fragment overlaps with the N-benzylpiperidine moiety of donepezil and is oriented toward CAS. Pyrimidine rings of **VB1** and **VB3** showed good overlap with the dihydroindenone part of donepezil. Surprisingly, **VB8** showed reverse orientation and its (prop-2-yn-1-yloxy)benzene fragment overlapped with the benzylpiperidine moiety of the donepezil aligned toward CAS of AChE. The 4-(2-phenoxyethyl)-morpholine moiety of **VB8** oriented toward 2,3-dihydroinden-1-one fragment of donepezil and accommodate in the PAS of AChE. The pyrimidine ring of **VB8** overlapped with the piperidine ring of donepezil, whereas the (prop-2-yn-1-yloxy)benzene fragment overlapped with the benzylic ring. Thus, altered orientation and additional interactions at the active site might be responsible for the high potency of **VB8** toward AChE enzyme.

Molecular Dynamics Simulation Studies. Molecular dynamics simulation (MD) were performed to study the protein$-$ligand interactions and to determine the thermodynamic stability of the docked compounds at the active pocket of the enzymes. The protein$-$ligand docked complexes of the most active compounds **VB1** with MAO-A and **VB8** with AChE were used for MD simulations. The MD simulation studies were conducted for 30 ns, and the interaction pattern of the test compound with different amino acids was analyzed. MD simulations yielded stable trajectories for **VB1** with MAO-Ain the first 20 ns, as noted by the time evolution of the potential energy and the root-mean-square deviation (RMSD) of the protein backbone, which ranged from 0.6 to 1.0 Å (Figure 9). There were no major structural alterations, and the pyrimidine moiety adopted similar orientation in the active site of MAO-A (Figure 9) as obtained during the docking studies. In particular, the 4-(2-phenoxyethyl)morpholine fragment of **VB1** was stacked against Tyr444 and Arg206. After the time

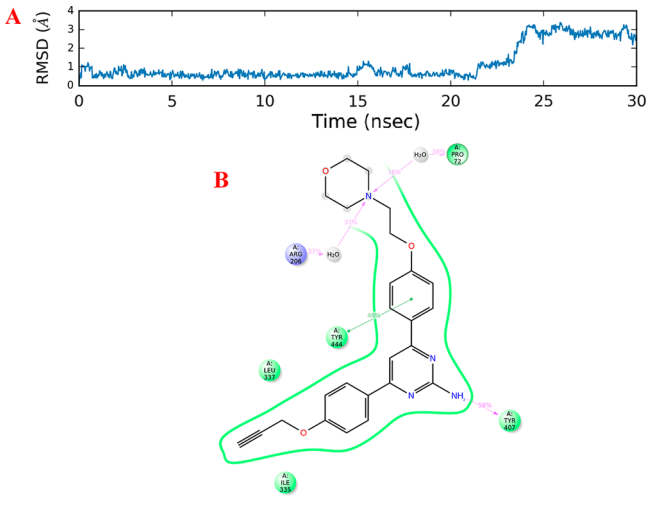

Figure 9. (A) RMSD graph of MD studies of **VB1** with MAO-A for 30 ns and (B) interactions of **VB1** with the active site residues of MAO-A after 30 ns MD simulation studies.

DOI: 10.1021/acschemneuro.8b00220
ACS Chem. Neurosci. 2019, 10, 252−265

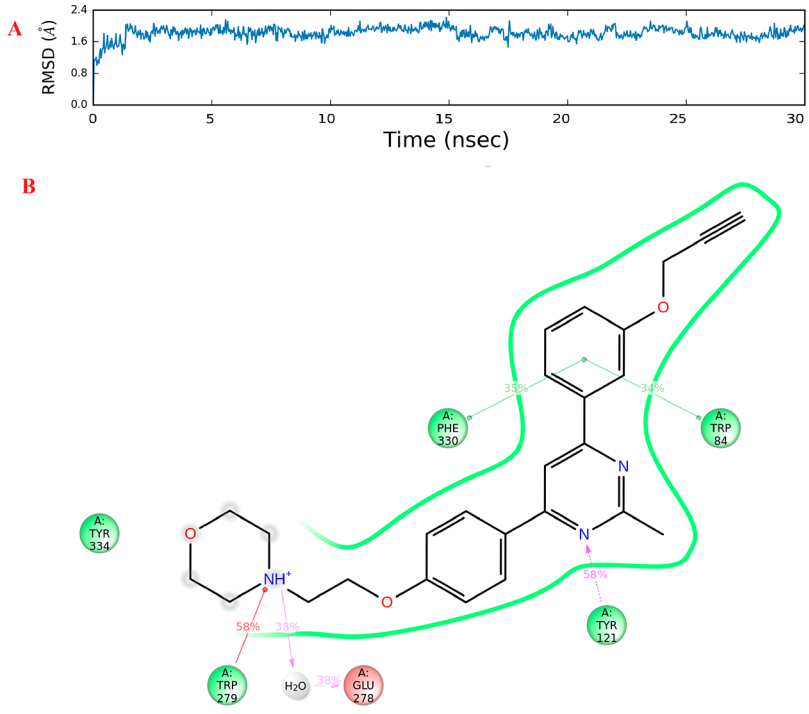

Figure 10. (A) RMSD graph of MD simulations studies of **VB8** with AChE for 30 ns and (B) interactions of **VB8** with the active site residues of AChE during 30 ns MD simulation studies.

Table 2. Physiochemical Properties of the Most Potent and Selective MAO-A and AChE Inhibitors[a]

name	mol. wt.	Log P	HB donor	HB acceptor	% human oral absorption	QPlogBB (optimum range −3.0−1.2)	BBB permeability predicted
VB1	430.505	3.94	3	8	96	−0.65	+ve
VB3	429.518	5.06	1	7	100	0.22	+ve
VB8	429.518	5.09	1	7	100	0.28	+ve

[a]+ve = high blood-brain barrier permeability, HB = hydrogen bond, QPlogBB = qualitatively predicted logarithmic ratio between the concentration of a compound in the brain and blood, LogP = partition coefficient of a molecule between an aqueous and lipophilic phase (octanol and water).

interval of 22 ns, there was a sudden hike in the RMSD, and thereafter, it showed stable trajectory up to 30 ns. RMSD oscillates in the range of 2 Å to 3 Å in this time interval. In the MD simulations studies it has been observed that **VB1** preserved most of the interactions observed during the docking studies. In addition, some new interactions with various amino acid residues were also observed (Figure 9). In the MD simulations, $\pi-\pi$ aromatic interaction with Tyr444 was retained. The NH_2 group present on the pyrimidine fragment move more toward Tyr407 and formed a hydrogen bond with it. The nitrogen atom of the morpholine ring formed hydrogen bonds with Pro72 and Arg206 through water bridge formation. It demonstrates the structural integrity of the MAO-A-VB1complex, and displayed similar binding features as done by clorgyline.

The MD simulations of AChE−**VB8** complex was performed to determine the binding stability of **VB8** at CAS and PAS of AChE. The complex yielded stable trajectories from 2 to 30 ns, as noted by the time evolution of the potential energy and the root-mean-square deviation (RMSD) of the protein backbone. The RMSD values for AChE−**VB8** complex ranged from 1.6 to 2.0 Å (Figure 10). For the initial 2 s, the RMSD value increase from 0.8 to 1.6, and thereafter it remained stable up to 30 ns. Analyzing the MD trajectory of AChE−**VB8** complex, it can be concluded that **VB8** showed strong tendency to be localized in the binding region of AChE. Nitrogen atom of the pyrimidine ring form hydrogen-bond with Tyr121. In the PAS of AChE, the protonated nitrogen atom of morpholine moiety maintained the initial cation−π interaction (from comparison of Figure 7 and Figure 10) throughout the MD simulations interval, indicating stable binding of **VB8** with AChE. In addition, the morpholine ring formed hydrogen bonding with the Glu278 residue through water bridge formation. The (prop-2-yn-1-yloxy)benzene fragment aligned toward CAS of AChE and showed aromatic $\pi-\pi$ interaction of **VB8** with Tyr330 and Trp84. The MD simulations of **VB8** does not indicate any abrupt local force that could potentially break up the inhibitor or can even delocalize it from the binding site of AChE. Thus, from the MD simulations studies of AChE-VB8complex, it can be concluded that the complex is stable and this stability might be responsible for the high *in vitro* potency of **VB8** for AChE.

ADME Properties. To determine the drug-like characteristics of the synthesized compounds, ADME parameters of these compounds were determined using Qikprop application of Schrodinger. **VB1** displayed very good drug-like profile with LogP value less than 5 and QPlogBB value as −0.65. In addition, **VB1** showed optimum oral absorption and blood-brain barrier permeability. **VB3** and **VB8** also showed 100% oral absorption and QPlogBB in the optimum range to cross the blood brain barrier (Table 2).

DOI: 10.1021/acschemneuro.8b00220
ACS Chem. Neurosci. 2019, 10, 252−265

SAR Studies. In the current studies, three different amidines have been used with R as $-NH_2$, $-CH_3$, or $-C_6H_5$ (Table 1). One ring of diphenylpyrimidines is optionally substituted with the morpholine or piperidine ethyl chain while other phenyl ring is functionalized with a propargyl group at ortho, meta, or para positions. The effect of different substituents on the activity is analyzed as reported in the Table 1. The compounds were evaluated for MAO-A, MAO-B, ee AChE, and eq BuChE inhibitory activities using enzymatic assays. All the compounds were found to be selective for MAO-A isoform with IC_{50} values in the nanomolar range and with moderate to very high selectivity index. It has been observed that the compounds with morpholine ethyl chain and propargyl group at para positions of both the phenyl rings showed high potency for MAO-A isoform and eeAChE. **VB1** with R as $-NH_2$ was found to be the most potent MAO-A inhibitor with an IC_{50} value of 18.34 nM, and it also showed potent ee AChE inhibitory activity with an IC_{50} value of 30.46 nM. **VB1** was also found to be the most potent BuChE inhibitor in the series with IC_{50} value of 0.666 ± 0.03 μM. **VB3** with R as −CH3 also showed strong inhibition potential against MAO-A and ee AChE with IC_{50} values of 28.33 and 18.92 nM, respectively. Replacement of -NH_2 with C_6H_5 in **VB2** reduces MAO-A activity by 5-fold. Shifting of propargyl group from para position to meta position (**VB7**) reduces MAO-A inhibitory activity by more than 12-fold, but there was no effect on the ee AChE inhibitory activity. Similarly, in **VB8**, meta propargyl group reduces MAO-A inhibitory activity by 35-fold when compared with **VB3**. However, **VB8** was found to be the most potent ee AChE inhibitor in the series with an IC_{50} value of 9.54 nM. In general, replacement of morpholine ring with the piperidine ring reduces MAO-A inhibitory activity (**VB4** and **VB5**). Shifting of morpholine substituent from para (**VB1**) to meta position (**VB12**) decreases MAO-A activity by 19-fold and ee AChE activity by 47-fold. It has been found that compounds with a propargyl substitution at the ortho and meta positions were less active toward MAO-A as compared with the para substituents. The current series of compounds displayed high selectivity index toward AChE as compared to BuChE (Table 1). **VB1** was found to be the most potent BuChE inhibitor, however, it showed SI of 22-fold for AChE. In the current series of compounds, VB8 displayed the highest SI of about 10^3 for AChE. Replacement of the amino group with methyl or phenyl groups (**VB2** and **VB3**) decreases BuChE inhibitory activity by about 22-fold. Shifting the propargyl group from para (**VB1**) to ortho (**VB9**) position drastically reduced the activity by about 240-fold. Similarly, shifting of morpholine ring from para (**VB1**) to meta position (**VB12**) decreases BuChE activity by 35-fold.Thus, **VB1**, **VB3**, and **VB8** were found to be the most promising compounds among the reported series of compounds.

CONCLUSIONS

AD is multifactorial in nature, and different enzymes including MAO, AChE, and amyloid beta are implicated in its pathogenesis. The pathomechanism of AD is complex in nature and single target drugs proved to be ineffective for the treatment of the disease. Thus, a multitarget directed approach is being explored for the development of effective drug candidates for the treatment of AD. A drug active on multiple targets may be characterized by an improved efficacy when compared with a highly selective pharmacological agent. Multitarget activities may potentiate efficacy either additively or synergistically and be less prone to the drug resistance. In the current study, a series of 4,6-diphenylpyrimidines has been rationally designed that can simultaneously target MAO enzymes and acetylcholinesterases for the treatment of AD. The phenyl rings were optionally substituted with a morpholine or piperidine ethyl chain and *O*-propargylated groups at ortho, meta, and para positions, and structure−activity relationship profile has been generated. Most of the compounds were found to be potent dual inhibitors of MAO-A isoform and AChE with IC_{50} values in nanomolar range. In the current series, **VB1** was found to be the most potent MAO-A and BuChE inhibitor with IC_{50} values of 18.34 ± 0.38 nM and 0.66 ± 0.03 μM. It also displayed potent AChE inhibitory activity with IC_{50} value of 30.46 ± 0.23 nM. **VB3** was another promising compound in the series with IC_{50} values of 28.33 ± 3.22 nM and 18.92 ± 0.29 nM against MAO-A and AChE, respectively. **VB8** was found to be the most potent AChE inhibitor with an IC_{50} value of 9.54 ± 0.07 nM and displayed very high SI (10^3) for AChE over BuChE. In the reversibility inhibition studies, **VB1**, **VB3**, and **VB8** were found to be reversible inhibitors of MAO-A and AChE. These compounds also displayed neuroprotective potential against 6-OHDA and H_2O_2 induced neurotoxicity in SH-SY5Y cells. Cytotoxicity studies were also performed with the three lead compounds using SH-SY5Y cell lines, and the compounds were found to be nontoxic even at 25 μM concentration. In the MD simulation studies of 30 ns, **VB1** and **VB8** were found to be stable in the active site of MAO-A and AChE, respectively. In the physicochemical evaluation studies, the most active compounds were found to possess drug-like characteristics with optimum oral absorption and good permeability to blood brain barrier. Thus, some of these dual acting compounds have the potential to be developed as drug candidates for the treatment of AD.[30]

EXPERIMENTAL SECTION

General Procedure for the Synthesis of 1 and 2. To hydroxy substituted acetophenone (0.5 g) or benzaldehydes (0.5 g), morpholine or piperidine ethyl chloride (1.2eq) was added in the presence of potassium carbonate as base (2.4eq) and acetone (30 mL) as solvent. The reaction mixture was refluxed for 12 h at 60 °C. The progress of reaction was monitored via TLC. After completion of the reaction, excess solvent was evaporated from the mixture using vacuum rotary evaporator. Then water (10 mL) was added, and the aqueous phase was extracted with ethyl acetate (10 mL × 3) washed with brine, dried over anhydrous Na_2SO_4, and the organic solvent was concentrated under vacuum using rotary evaporator.

General Procedure for the Synthesis of 3. To a mixture of **1** (1 equiv) and **2** (1 equiv) in methanol (20 mL), aqueous sodium hydroxide (20%) was added slowly with continuous stirring. The reaction mixture was stirred for 3 h at room temperature. The completion of the reaction was monitored via TLC. After completion of the reaction, excess solvent was evaporated from the mixture using a rotary evaporator. Chilled water was poured into the reaction mixture, and precipitates of **3** were filtered and dried.

General Procedure for the Synthesis of VB1−VB15. To a mixture of **3** (500 mg) and amidine (1.2 equiv), anhydrous sodium carbonate (2.4 equiv) was added in acetonitrile (5 mL) as solvent. The reaction mixture was refluxed for 24 h at 85 °C. The progress of the reaction was monitored via TLC. After completion of the reaction, excess solvent was evaporated under vacuum using rotary evaporator. Then water (10 mL) was added, and the aqueous phase was extracted with ethyl acetate (3 × 10 mL), washed with brine, dried over anhydrous Na_2SO_4, and the organic solvent was concentrated under vacuum using rotary evaporator and purified via column chromatog-

DOI: 10.1021/acschemneuro.8b00220
ACS Chem. Neurosci. 2019, 10, 252−265

raphy (EtOAc:Pet ether). The final products were characterized by NMR spectroscopy and HRMS.

Spectral Analysis. *4-(4-(2-Morpholinoethoxy)phenyl)-6-(4-(prop-2-yn-1-yloxy)phenyl)pyrimidin-2-amine (**VB1**).* Yield 59%, ^{1}H NMR ($CDCl_3$, 400 MH_Z, δ with TMS = 0): 8.05−8.00 (4H, m), 7.35 (1H, s), 7.07 (2H, d, J = 8 Hz), 6.99 (2H, d, J = 8 Hz), 5.16 (2H, s), 4.76 (2H, d, J = 2.4 Hz), 4.18 (2H, t, J = 4 Hz), 3.75 (4H, t, J = 4 Hz), 2.83 (2H, t, J = 4 Hz), 2.60 (4H, t, J = 4 Hz), 2.55 (1H, t, J = 2.4 Hz), ^{13}C NMR ($CDCl_3$, 100 MH_Z, δ with TMS = 0)δ: 165.40, 165.28, 163.49, 160.71, 159.41, 131.13, 130.36, 128.36, 128.58, 115.00, 114.70, 102.86, 78.19, 75.89, 66.93, 65.89, 57.58, 55.85, 54.13 **HRMS**: for $C_{25}H_{26}N_4O_3$, calculated $[M + H]^+$: 431.2083; observed $[M + H]^+$: 431.2060

*4-(2-(4-(2-Phenyl-6-(4-(prop-2-yn-1-yloxy)phenyl)pyrimidin-4-yl)phenoxy)ethyl)morpholine (**VB2**).* Yield 63%, ^{1}H NMR ($CDCl_3$, 400 MH_Z, δ with TMS = 0): 8.68 (2H, d, J = 8 Hz), 8.24 (4H, t, J = 8 Hz), 7.86 (1H, s), 7.53−7.49 (3H, m), 7.12 (2H, d, J = 8 Hz), 7.04 (2H, d, J = 8 Hz), 4.77 (2H, d, J = 2.4 Hz), 4.19 (2H, t, J = 4 Hz), 3.75 (4H, t, J = 4 Hz), 2.84 (2H, t, J = 4 Hz), 2.60 (4H, t, J = 4 Hz), 2.56 (1H, t, J = 2.4 Hz), ^{13}C NMR ($CDCl_3$, 100 MH_Z, δ with TMS = 0)δ: 164.01, 163.89, 161.02, 159.73, 138.40, 130.59, 130.28, 128.83, 128.48, 115.20, 114.89, 108.75, 78.19, 75.89, 66.99, 65.93, 57.66, 55.95, 54.20 **HRMS**: for $C_{31}H_{29}N_3O_3$, calculated $[M + H]^+$: 492.2287; observed $[M + H]^+$: 492.2271

*4-(2-(4-(2-Methyl-6-(4-(prop-2-yn-1-yloxy)phenyl)pyrimidin-4-yl)phenoxy)ethyl)morpholine (**VB3**).* Yield 58%, ^{1}H NMR ($CDCl_3$, 400 MH_Z, δ with TMS = 0): 8.11−8.07 (4H, m), 7.76 (1H, s), 7.10 (2H, d, J = 8 Hz), 7.02 (2H, d, J = 8 Hz), 4.77 (2H, d, J = 2.4 Hz), 4.19 (2H, t, J = 4 Hz), 3.75 (4H, t, J = 4 Hz), 2.84 (2H, t, J = 4 Hz), 2.81 (3H, s), 2.61 (2H, t, J = 4 Hz), 2.56 (1H, t, J = 2.4 Hz), ($CDCl_3$, 100 MH_Z, δ with TMS = 0)δ: 168.32, 164.07, 163.96, 160.85, 159.55, 130.94, 130.17, 128.72, 115.18, 114.87, 108.49, 78.13, 75.93, 66.91, 65.90, 57.57, 55.87, 54.13, 26.53 **HRMS**: for $C_{26}H_{27}N_3O_3$, calculated $[M + H]^+$: 430.2131; observed $[M + H]^+$: 430.2079

*2-Phenyl-4-(4-(2-(piperidin-1-yl)ethoxy)phenyl)-6-(4-(prop-2-yn-1-yloxy)phenyl)pyrimidine (**VB4**).* Yield 61%, ^{1}H NMR ($CDCl_3$, 400 MH_Z, δ with TMS = 0): 8.69 (2H, dd, J_1 = 8 Hz, J_2 = 4 Hz), 8.23 (4H, t, J = 8 Hz), 7.84 (1H, s), 7.52−7.42 (3H, m) 7.11 (2H, d, J = 8 Hz), 7.03 (2H, d, J = 8 Hz), 4.76 (2H, d, J = 2.4 Hz), 4.19 (2H, t, J = 4 Hz), 2.82 (2H, t, J = 4 Hz), 2.57−2.55 (5H, m), 1.66−1.60 (4H,m) 1.46 (2H, bd), ($CDCl_3$, 100 MH_Z, δ with TMS = 0)δ: 164.26, 164.04, 163.82, 161.12, 159.70, 138.43, 131.04, 130.56, 130.11, 128.80, 128.71, 128.48, 115.18, 114.89, 108.71, 78.26, 76.04, 66.02, 57.83, 55.94, 55.14, 29.81, 25.88, 24.19 **HRMS**: for $C_{32}H_{31}N_3O_2$, calculated $[M + H]^+$: 490.2495; observed $[M + H]^+$: 490.2470

*2-Methyl-4-(4-(2-(piperidin-1-yl)ethoxy)phenyl)-6-(4-(prop-2-yn-1-yloxy)phenyl)pyrimidine (**VB5**).* Yield 67%,^{1}H NMR ($CDCl_3$, 400 MH_Z, δ with TMS = 0): 8.07 (4H, t, J = 8 Hz), 7.74 (1H, s), 7.08 (2H, d, J = 8 Hz), 7.00 (2H, d, J = 8 Hz), 4.75 (2H, d, J = 4 Hz), 4.17 (2H, t, J = 4 Hz), 2.82−2.79 (5H, m), 2.53 (4H, b), 1.61 (4H, b), 1.44 (2H, b), 1.23 (1H, b), ($CDCl_3$, 100 MH_Z, δ with TMS = 0)δ: 168.35, 164.18, 163.98, 161.03, 159.59, 131.01, 130.79, 130.35, 130.11, 130.06, 129.47, 128.77, 115.33, 115.23, 114.95, 108.53, 78.21, 76.01, 66.07, 57.85, 55.92, 55.13, 29.79, 25.89, 24.17, **HRMS**: for $C_{27}H_{29}N_3O_2$, calculated $[M + H]^+$: 428.2338; observed $[M + H]^+$: 428.2293

*4-(2-(4-(2-Phenyl-6-(3-(prop-2-yn-1-yloxy)phenyl)pyrimidin-4-yl)phenoxy)ethyl)morpholine (**VB6**).* Yield 62%,^{1}H NMR ($CDCl_3$, 400 MH_Z, δ with TMS = 0): 8.70 (2H, dd, J_1 = 8 Hz, J_2 = 4 Hz), 8.25 (2H, d, J = 8 Hz), 7.97 (1H,s), 7.91 (1H,s), 7.86, (1H, d, J = 8 Hz), 7.54−7.56 (4H, m), 7.15 (1H, dd, J_1 = 8 Hz, J_2 = 4 Hz), 7.06 (2H, d, J = 8 Hz), 4.82 (2H, d, J = 4 Hz), 4.20 (2H, t, J = 4 Hz), 3.76 (4H, t, J = 4 Hz), 2.85 (2H, t, J = 4 Hz), 2.60 (5H, m), ($CDCl_3$, 100 MH_Z, δ with TMS = 0)δ: 164.37, 164.27, 164.06, 161.13, 158.17, 139.32, 138.25, 130.70, 130.10, 130.01, 128.88, 128.51, 120.50, 117.11, 114.93, 113.99, 109.61, 78.50, 75.94, 67.01, 65.98, 57.65, 56.13, 54.21, **HRMS**: for $C_{31}H_{29}N_3O_3$, calculated $[M + H]^+$: 492.2287; observed $[M + H]^+$: 492.2256

*4-(4-(2-Morpholinoethoxy)phenyl)-6-(3-(prop-2-yn-1-yloxy)-phenyl)pyrimidin-2-amine (**VB7**).* Yield 59%,^{1}H NMR ($CDCl_3$, 400 MH_Z, δ with TMS = 0): 8.00 (2H, d, J = 8 Hz), 7.90 (1H, dd, J_1 = 8 Hz, J_2 = 4 Hz), 7.65 (1H, m), 7.39 (1H, t, J = 8 Hz), 7.36 (1H, s), 7.08 (1H, dd, J_1 = 8 Hz, J_2 = 4 Hz), 6.98 (2H, d, J = 8 Hz), 6.90 (1H, t, J = 8 Hz), 5.22 (2H, s), 4.77 (2H, d, J = 4 Hz), 4.16 (4H, t, J = 4 Hz), 3.73 (2H, t, J = 4 Hz), 2.82 (4H, t, J = 4 Hz), 2.53 (2H, b), ($CDCl_3$, 100 MH_Z, δ with TMS = 0)δ: 165.71, 163.56, 160.86, 158.01, 139.49, 130.69, 129.89, 128.70, 120.44, 117.08, 114.79, 114.48, 114.29, 113.53, 103.73, 78.49, 75.82, 66.97, 65.93, 57.63, 56.04, 54.18, **HRMS**: for $C_{25}H_{26}N_4O_3$, calculated $[M + H]^+$: 431.2083; observed $[M + H]^+$: 431.2060

*4-(2-(4-(2-Methyl-6-(3-(prop-2-yn-1-yloxy)phenyl)pyrimidin-4-yl)phenoxy)ethyl)morpholine (**VB8**).* Yield 59%,^{1}H NMR ($CDCl_3$, 400 MH_Z, δ with TMS = 0): 8.08 (2H, d, J = 8 Hz), 7.78 (1H, m), 7.72−7.69 (2H, m), 7.43 (1H, t, J = 8 Hz), 7.10 (1H, d, J = 8 Hz), 7.01 (2H, t, J = 8 Hz), 4.78 (2H, d, J = 4 Hz), 4.18 (2H, t, J = 4 Hz), 3.74 (4H, t, J = 4 Hz), 2.83 (2H, t, J = 4 Hz), 2.83 (3H, s), 2.59 (4H, t, J = 4 Hz), 2.54 (1H, t, J = 4 Hz), ($CDCl_3$, 100 MH_Z, δ with TMS = 0)δ: 168.50, 164.37, 164.29, 161.01, 158.14, 139.31, 131.03, 130.07, 128.83, 120.56, 117.13, 114.97, 113.77, 109.45, 78.44, 75.84, 66.98, 65.97, 57.64, 56.08, 54.20, 29.79, **HRMS**: for $C_{26}H_{27}N_3O_3$, calculated $[M + H]^+$: 430.2131; observed $[M + H]^+$: 430.2086

*4-(4-(2-Morpholinoethoxy)phenyl)-6-(2-(prop-2-yn-1-yloxy)-phenyl)pyrimidin-2-amine (**VB9**).* Yield 55%,^{1}H NMR ($CDCl_3$, 400 MH_Z, δ with TMS = 0): 8.00 (2H, d, J = 8 Hz), 7.85 (1H, dd, J_1 = 8 Hz, J_2 = 4 Hz), 7.60 (1H, m), 7.40 (1H, dd, J_1 = 8 Hz, J_2 = 4 Hz), 7.12 (2H, t, J = 8 Hz), 6.97 (2H, d, J = 8 Hz), 5.12 (2H, s), 4.75 (2H, d, J = 4 Hz), 4.16 (2H, t, J = 4 Hz), 3.73 (4H, t, J = 4 Hz), 2.82 (2H, t, J = 4 Hz), 2.59 (4H, b), 2.52 (1H, t, J = 4 Hz), ($CDCl_3$, 100 MH_Z, δ with TMS = 0)δ: 164.69, 164.30, 163.39, 160.70, 155.69, 130.94, 128.81, 122.22, 114.70, 114.16, 113.54, 109.19, 108.56, 78.53, 75.92, 66.99, 65.92, 57.66, 56.69, 54.18, **HRMS**: for $C_{25}H_{26}N_4O_3$, calculated $[M + H]^+$: 431.2083; observed $[M + H]^+$: 431.2036

*4-(2-(4-(2-Phenyl-6-(2-(prop-2-yn-1-yloxy)phenyl)pyrimidin-4-yl)phenoxy)ethyl)morpholine (**VB10**).* Yield 63%,^{1}H NMR ($CDCl_3$, 400 MH_Z, δ with TMS = 0): 8.67 (1H, dd, J_1 = 8 Hz, J_2 = 4 Hz), 8.27 (1H, s), 8.26 (2H, d, J = 8 Hz), 7.53−7.44 (4H, m), 7.21 (1H, t, J = 8 Hz), 7.13 (1H, d, J = 8 Hz), 7.04 (2H, d, J = 8 Hz), 4.80 (2H, d, J = 4 Hz), 4.19 (2H, t, J = 4 Hz), 3.75 (4H, t, J = 4 Hz), 2.84 (2H, t, J = 4 Hz), 2.60 (4H, b), 2.56 (1H, t, J = 4 Hz), ($CDCl_3$, 100 MH_Z, δ with TMS = 0)δ: 164.19, 163.29, 162.79, 160.97, 156.23, 138.60, 131.59, 131.33, 130.56, 130.40, 128.97, 128.44, 128.41, 126.56, 122.35, 114.86, 114.72, 113.53, 78.50, 76.00, 67.02, 66.05, 57.68, 56.82, 54.22, **HRMS**: for $C_{31}H_{29}N_3O_3$, calculated $[M + H]^+$: 492.2287; observed $[M + H]^+$: 492.2256

*4-(2-(3-(2-Phenyl-6-(4-(prop-2-yn-1-yloxy)phenyl)pyrimidin-4-yl)phenoxy)ethyl)morpholine (**VB11**).* Yield 62%,^{1}H NMR ($CDCl_3$, 400 MH_Z, δ with TMS = 0): 8.68 (2H, dd, J_1 = 8 Hz, J_2 = 4 Hz), 8.26 (2H, dd, J_1 = 8 Hz, J_2 = 4 Hz), 7.90 (1H, d, J = 8 Hz), 7.85 (1H, s), 7.81 (1H, d, J = 8 Hz), 7.54−7.50 (3H, m), 7.44 (1H, d, J = 8 Hz), 7.13 (2H, dd, J_1 = 8 Hz, J_2 = 4 Hz), 7.01 (1H, dd, J_1 = 8 Hz, J_2 = 4 Hz), 4.78 (2H, d, J = 4 Hz), 4.26 (2H, t, J = 4 Hz), 3.77 (4H, t, J = 4 Hz), 2.90 (2H, t, J = 4 Hz), 2.67 (4H, b), 2.56 (1H, t, J = 4 Hz), ($CDCl_3$, 100 MH_Z, δ with TMS = 0)δ: 166.67, 163.80, 161.95, 160.94, 147.89, 138.06, 130.75, 129.60, 128.88, 128.62, 128.42, 119.49, 116.86, 114.91, 114.58, 112.04, 110.66, 80.96, 76.80, 71.58, 66.75, 65.72, 57.56, 54.09, **HRMS**: for $C_{31}H_{29}N_3O_3$, calculated $[M + H]^+$: 492.2287; observed $[M + H]^+$: 492.2256

*4-(3-(2-Morpholinoethoxy)phenyl)-6-(4-(prop-2-yn-1-yloxy)-phenyl)pyrimidin-2-amine (**VB12**).* Yield 72%, ^{1}H NMR ($CDCl_3$, 400 MH_Z, δ with TMS = 0): 8.01 (2H, d, J = 8 Hz), 7.60 (1H, s), 7.57 (1H, d, J = 8 Hz), 7.36 (2H, t, J = 8 Hz), 7.04 (2H, d, J = 12 Hz), 7.00 (1H, d, J = 8 Hz), 5.35 (2H, s), 4.73 (2H, d, J = 2.4 Hz), 4.18 (2H, t, J = 4 Hz), 3.73 (4H, t, J = 4 Hz), 2.82 (2H, t, J = 4 Hz), 2.59 (4H, t, J = 4 Hz), 2.54 (1H, t, J = 2.4 Hz), ($CDCl_3$, 100 MH_Z, δ with TMS = 0)δ: 165.71, 163.56, 160.86, 158.01, 139.49, 130.69, 129.89, 128.70, 120.44, 117.08, 114.79, 114.48, 114.29, 113.53, 103.73, 78.49, 75.82, 66.97, 65.93, 57.63, 56.04, 54.18, **HRMS**: for $C_{25}H_{26}N_4O_3$, calculated $[M + H]^+$: 431.2083; observed $[M + H]^+$: 431.2018

DOI: 10.1021/acschemneuro.8b00220
ACS Chem. Neurosci. 2019, 10, 252−265

*4-(2-(3-(2-Methyl-6-(4-(prop-2-yn-1-yloxy)phenyl)pyrimidin-4-yl)phenoxy)ethyl)morpholine (**VB13**).* Yield 54%, ^{1}H NMR ($CDCl_3$, 400 MH_Z, δ with TMS = 0): 8.09 (2H, d, J = 8 Hz), 7.78 (1H, s), 7.64 (1H, d, J = 8 Hz), 7.51−7.47 (1H, m), 7.38 (1H, t, J = 8 Hz), 7.07 (2H, d, J = 12 Hz), 7.02 (1H, dd, J_1 = 8 Hz, J_2 = 4 Hz), 4.74 (2H, d, J = 4 Hz), 4.28 (2H, t, J = 4 Hz), 4.19 (2H, t, J = 4 Hz), 3.72 (4H, t, J = 4 Hz), 2.81 (3H, s), 2.59 (4H, t, J = 4 Hz), 2.54 (1H, t, J = 2.4 Hz), ($CDCl_3$, 100 MH_Z, δ with TMS = 0)δ: 168.47, 164.44, 164.25, 159.72, 159.33, 139.14, 131.02, 130.02, 128.91, 128.83, 118.83, 116.96, 115.27, 113.29, 109.49, 78.18, 76.07, 66.98, 65.88, 65.66, 57.75, 55.92, 54.17, **HRMS**: for $C_{26}H_{27}N_3O_3$, calculated $[M + H]^+$: 430.2131; observed $[M + H]^+$: 430.2101

*2-Phenyl-4-(4-(2-(piperidin-1-yl)ethoxy)phenyl)-6-(3-(prop-2-yn-1-yloxy)phenyl)pyrimidine (**VB14**).* Yield 53%, ^{1}H NMR ($CDCl_3$, 400 MH_Z, δ with TMS = 0): 8.70 (2H, dd, J_1 = 8 Hz, J_2 = 4 Hz), 8.24 (2H, d, J = 8 Hz), 7.96 (1H, t, J = 8 Hz), 7.91 (1H, s), 7.85 (1H, dd, J_1 = 8 Hz, J_2 = 4 Hz), 7.53−7.45 (4H, m), 7.13 (1H, dd, J_1 = 8 Hz, J_2 = 4 Hz), 7.05 (2H, d, J = 8 Hz), 4.81 (2H, d, J = 8 Hz), 4.20 (2H, t, J = 4 Hz), 2.83 (2H, t, J = 4 Hz), 2.58 (4H, t, J = 4 Hz), 1.66−1.60 (4H, m), 1.47−1.40 (3H, m), ($CDCl_3$, 100 MH_Z, δ with TMS = 0)δ: 164.35, 164.37, 164.05, 161.16, 158.17, 139.36, 138.29, 130.70, 130.01, 128.85, 128.51, 120.52, 117.11, 114.56, 113.96, 109.61, 78.39, 75.83, 57.92, 56.16, 75.83, 29.72, 25.86, 24.13, **HRMS**: for $C_{32}H_{31}N_3O_2$, calculated $[M + H]^+$: 490.2495; observed $[M + H]^+$: 490.2480

*4-(4-(2-(Piperidin-1-yl)ethoxy)phenyl)-6-(3-(prop-2-yn-1-yloxy)-phenyl)pyrimidin-2-amine (**VB15**).* Yield 58%, ^{1}H NMR ($CDCl_3$, 400 MH_Z, δ with TMS = 0): 7.99 (2H, d, J = 8 Hz), 7.65−7.62 (2H, m), 7.39 (1H, t, J = 8 Hz), 7.35 (1H, s), 7.08 (1H, dd, J_1 = 8 Hz, J_2 = 4 Hz), 6.97 (2H, d, J = 8 Hz), 5.26 (2H, s), 4.75 (2H, d, J = 4 Hz), 4.16 (2H, t, J = 4 Hz), 2.80 (2H, t, J = 4 Hz), 2.53 (5H, b), 1.62−1.58 (4H, m), 0.97−0.92 (2H, m), ($CDCl_3$, 100 MH_Z, δ with TMS = 0)δ: 165.75, 165.55, 163.60, 160.96, 158.07, 139.53, 131.02, 129.87, 128.67, 120.45, 117.08, 114.79, 113.50, 103.68, 78.51, 75.83, 66.01, 57.85, 56.03, 55.11, 25.87, 34.17, **HRMS**: for $C_{26}H_{28}N_4O_2$, calculated $[M + H]^+$: 429.2291; observed $[M + H]^+$: 429.2238

*(E)-1-(4-(2-Morpholinoethoxy)phenyl)-3-(4-(prop-2-yn-1-yloxy)-phenyl)prop-2-en-1-one (**3a**).* Yield 85%, ^{1}H NMR ($CDCl_3$, 400 MH_Z, δ with TMS = 0):8.01 (2H, d, J = 8 Hz), 7.66 (1H, d, J = 16 Hz), 7.60 (2H, d, J = 8 Hz), 7.43 (1H, d, J = 16 Hz), 7.02−6.95 (4H, m), 4.73 (2H, d, J = 4 Hz), 4.18 (2H, t, J = 4 Hz), 3.73 (4H, t, J = 4 Hz), 2.83 (2H, t, J = 4 Hz), 2.58 (2H, t, J = 4 Hz), 2.55 (1H, t, J = 4 Hz), ^{13}C NMR ($CDCl_3$, 100 MH_Z, δ with TMS = 0): 188.72, 162.50, 159.37, 143.68, 131.45, 130.80, 130.12, 128.68, 120.01, 115.34, 114.42, 77.46, 76.12, 66.99, 66.09, 57.55, 55.90, 54.19 **MS**: for $C_{24}H_{25}NO_4$, calculated $[M]^+$: 391.17; observed $[M]^+$: 391

*(E)-1-(4-(2-Morpholinoethoxy)phenyl)-3-(2-(prop-2-yn-1-yloxy)-phenyl)prop-2-en-1-one (**3b**).* Yield 83%, ^{1}H NMR ($CDCl_3$, 400 MH_Z, δ with TMS = 0): 8.02−8.09 (3H, m), 7.63−7.69 (2H, m), 7.34 (1H, t, J = 8H_Z), 7.03 (2H, t, J = 8H_Z), 6.96 (2H, d, J = 8H_Z), 4.79 (2H, d, J = 2.4 H_Z), 4.18 (2H, t, J = 4H_Z), 3.73 (4H, t, J = 4H_Z), 2.82 (2H, t, J = 4H_Z), 2.56 (4H, t, J = 4H_Z), 2.55 (1H, t, J = 4H_Z), ^{13}C NMR ($CDCl_3$, 100 MH_Z, δ with TMS = 0)δ: 189.25, 162.48, 156.72, 139.33, 131.39, 130.93, 129.57, 124.76, 123.17, 121.77, 114.38, 112.80, 78.14, 76.07, 66.99, 66.06, 57.55, 56.26, 54.18 **MS**: for $C_{24}H_{25}NO_4$, calculated $[M]^+$: 391.17; observed $[M]^+$: 391

*(E)-1-(3-(2-Morpholinoethoxy)phenyl)-3-(4-(prop-2-yn-1-yloxy)-phenyl)prop-2-en-1-one (**3c**).* Yield 87%, ^{1}H NMR ($CDCl_3$, 400 MH_Z, δ with TMS = 0): 7.76 (1H, d, J = 16 Hz), 7.58 (3H, t, J = 8 Hz), 7.52 (1H, s), 7.40−7.36 (2H, m), 7.11 (1H, d, J = 8 Hz), 7.00 (2H, dd, J_1 = 8 Hz, J_2 = 4 Hz), 4.72 (2H, t, J = 4 Hz), 3.72 (4H, t, J = 4 Hz), 2.81 (2H, t, J = 4 Hz), 2.57 (4H, b), 2.54 (1H, t, J = 4 Hz), ^{13}C NMR ($CDCl_3$, 100 MH_Z, δ with TMS = 0)δ: 190.25, 159.57, 159.07, 144.61, 139.86, 130.27, 129.66, 128.47, 121.23, 120.23, 119.70, 115.39, 113.67, 78.06, 76.15, 66.97, 65.95, 57.67, 55.91, 54.15 **MS**: for $C_{24}H_{25}NO_4$, calculated $[M]^+$: 391.17; observed $[M]^+$: 391

BIOLOGICAL STUDIES

Determination of hMAO Inhibition Activity. The synthesized compounds were evaluated against MAO-A and MAO-B isoforms for their inhibitory potential using Amplex Red assay kit through fluorimetric method described by us and others.[23]

Briefly, 100 μL of sodium phosphate buffer (0.05 M, pH 7.4) containing the test drug and reference inhibitors, in various concentrations along with adequate amounts of recombinant hMAO (hMAO-A: 1.1 μg protein; specific activity: 150 nmol of p-tyramine oxidized to p-hydroxyphenylacetaldehyde/min/mg protein; hMAO-B: 7.5 μg of protein; specific activity: 22 nmol of p-tyramine transformed/min/mg protein) enzyme, were incubated for 15 min at 37 °C in a flat-black-bottom 96-well plates (Tarsons) in a incubator. After the incubation period, the reaction was started by adding (final concentrations) 200 μM Amplex Red reagent, 1 U/mL horseradish peroxidase and 1 mM p-tyramine. After 30 min of incubation in the dark, the production of H_2O_2 was quantified at 37 °C in a multidetection microplate fluorescence reader (Synergy^{HI}, Bio-Tek Instruments) based on the fluorescence generated at excitation wavelength of 545 nm and emission wavelength of 590 nm. Control experiments were carried out simultaneously by replacing the test drug with the vehicle. A direct reaction of test drug with the Amplex Red reagent in a sodium phosphate buffer was performed to minimize the possibility of the test drugs to influence the fluorescence generated in the reaction mixture due to nonenzymatic inhibition. However, no significant modulation in the fluorescence was observed. The specific final fluorescence emission was calculated after subtraction of the background activity determined from vials containing all the components except the hMAO enzymes replaced by a sodium phosphate buffer solution.

Acetylcholinesterase Inhibition Assay. Acetylcholinesterase inhibition activity was determined using Amplex Red Acetylcholine/Acetylcholinesterase assay kit (A12217) purchased from the Molecular Probes, Inc./Invitrogen.[38] Briefly, 100 μL of Tris-HCl buffer (0.05 M, pH 8.0) containing the synthesized test drugs and reference inhibitors, in various concentrations along with adequate amounts of recombinant AChE (0.2U/mL) enzyme, were incubated for 15 min at 37 °C in a flat-black-bottom 96-well plates (Tarsons). Reaction was started by adding 100 μL of working solution of 400 μM Amplex Red reagent containing 2 U/mL horseradish peroxidase, 0.2 U/mL choline oxidase, and 100 μM acetylcholine. After 30 min of incubation in the dark, the production of H_2O_2 and subsequent formation of resorufin from Amplex red dye was quantified at 37 °C in a multidetection microplate fluorescence reader (Synergy^{HI}, Bio-Tek Instruments) based on the fluorescence generated at excitation wavelength of 545 nm and emission wavelength of 590 nm. A positive control experiment was carried out simultaneously by replacing the test drugs with the vehicle. A second positive control was carried out by using 20 mM H_2O_2. A 1× reaction buffer without acetylcholinesterase was used as negative control. The specific final fluorescence emission was calculated after subtraction of the background activity, determined from wells containing all components except the AChE replaced by a 1× buffer solution. Each experiment was performed in triplicate (n = 3).

BuChE Inhibition Assay. The procedure described by Ellman et al. was used for BuChE inhibition assays with minor modifications.[39] BuChE was purchased from sigma Aldrich (CAS No. 9001-80-5). Butyrylthiocholine iodide (BTCI), 5.5′-dithiobis (2-nitrobenzoic acid) (DTNB − Ellman's reagent) were purchased from Himedia. The assays were performed in

DOI: 10.1021/acschemneuro.8b00220
ACS Chem. Neurosci. 2019, 10, 252−265

tris-HCl buffer (pH-8) and donepezil was used as standard compound. Six different concentrations of 20, 10, 1, 0.1, 0.01, and 0.001 μM of test compound were used to determine the IC_{50} values. Both 50 μL (0.6 Uml^{-1}) and 20 μL of test or standard compounds were incubated in 96-well plates for 30 min. Next, 100 μL (1.5 mM) of DTNB was added in the above solution. The substrate, that is, BTCI (30 mM, 10 μL), was added into it, and the absorbance was recorded immediately at 415 nm for 20 at 1 min interval using Biotek well plate reader. The IC_{50} values were calculated using absorbance obtained from the test and standard compounds. The assays were performed in triplicate and in three independent runs.

Reversibility Inhibition Studies. For reversibility inhibition studies, the protocol was adopted from the literature.[30,31] Briefly, the test inhibitors were incubated with the MAO enzymes at concentrations of 10 × IC_{50} and 100 × IC_{50} at 37 °C for 30 min (negative control performed in the absence of inhibitor), and 4% DMSO was added as cosolvent to all incubations. After a 30 min incubation period, the samples were subsequently diluted to 100-fold with the addition of tyramine substrate to achieve final inhibitor concentrations of 0.1 × IC_{50} and 1 × IC_{50} value, respectively. As positive controls, MAO-A and MAO-B were incubated with the irreversible inhibitors, clorgyline and pargyline, respectively, at 10 × IC_{50} concentrations and then diluted 100-fold to achieve final inhibitor concentrations of 0.1 × IC_{50}. The residual MAO activities after dilutions were measured (n = 3), and the residual enzyme activities were expressed as mean ± SD.

ROS Production Inhibition Studies. Intracellular levels of ROS were determined using protocol described elsewhere,[40] using nonfluorescent compound 2′,7′-dichlorofluorescein diacetate (DCF-DA). It is permeable to the cell membrane, where it is hydrolyzed by intracellular esterases and further oxidized by ROS to a fluorescent compound 2′,7′-DCF. Cells (SH-SY5Y) were seeded in 96-well plates (1×10^4 cells/well) and left for 24 h in complete media at 37 °C. Then media was removed, washed with PBS, and cells were treated with the test compounds (without FBS) for 24 h at different concentrations (1, 5, and 25 μM). After completion of the experiment, cells were rinsed with PBS thrice and then treated with H_2DCF-DA (50 μM) and incubated for 30 min at 37 °C. Following incubation, cells were rinsed with PBS, and fluorescence was detected at wavelength of 478 nm excitation and 518 nm emission.

Neuroprotective Studies. The neuroprotective potential of compounds was determined against 6-OHDA neurotoxin using MTT assay.[41] For this assay, SH-SY5Y cells were plated in 96 wells, at 10^6 cells/well density. The cells were cultured for 24 h in DMEM/F-12 media containing 10% FBS and horse serum supplemented 1% penicillin and streptomycin antibiotic solution. Then cells were treated with the target compounds (at concentrations of 1−25 μM), 4 h before 6-OHDA (12.5 μM). After 24 h of incubation in the oven, at 37 °C and a 5% CO_2, 95% O_2 atmosphere, the tested compounds were replaced with 80 mL of medium and 20 mL of MTT in PBS (0.5 mg/mL, final concentration). The cells were incubated for another 4 h. After the removal of MTT, the formazan crystals were dissolved in DMSO. The amount of formazan was measured using a microculture plate reader with a test wavelength of 570 nm. Results were expressed as the mean ± SD of three independent experiments.

Cytotoxicity Studies. With an aim to test the cytotoxicity of the synthesized compounds on neuronal cells, MTT assays were carried out with human neuroblastoma SH-SY5Y cells.[23] Approximately 10 000 cells were seeded per well of a 96-well plate in DMEM/F-12 media containing 10% FBS and horse serum supplemented 1% penicillin and streptomycin antibiotic solution for 24 h and treated as indicated in the experimental design. Cells were treated with synthesized compounds at concentrations of 1, 5, and 25 μM for 24 h in a humidified CO_2 incubator, maintained at 37 °C with 5% CO_2 and 95% humidity under serum-free conditions.

Metal-Chelating Study. Metal-chelating studies were performed with a UV−vis spectrophotometer. The absorption spectra of each compound (50 μM, final concentration) alone or in the presence of $CuSO_4$, $FeSO_4$, and $FeCl_3$ (50 μM, final concentration) for 30 min in 20% (v/v) methanol/buffer (20 mM HEPES, 150 mM NaCl, pH = 7.4) were recorded at room temperature.[42]

Kinetic Studies of AChE Inhibition. To determine the mechanism of action of the most potent inhibitor of AChE, **VB8**, kinetic study was performed using ee AChE with the help of earlier reported protocols.[25,43] A Lineweaver−Burk double reciprocal graph was plotted at different concentrations of substrate ACh (0.1 mM−1 mM) by using the same methodology reported for the *in vitro* inhibition study of AChE. Progress curves were analyzed by steady state turnover of substrate, and values of linear regression were fitted according to Lineweaver−Burk replots using excel software (2016). Three concentrations of VB8 (1, 10, and 100 nM) were used for kinetic study. The plots were assessed by weighted least-squares analysis that assumed the variance of ν to be constant for whole data set. Slopes of the reciprocal of ν were then plotted against the reciprocal of the substrate concentration.

Molecular Docking Studies. Docking studies can provide some valuable information on the ligand's orientation and its interactions at the receptor site. To determine the mode of interaction of the synthesized ligands at the active site of hMAO-A and AChE enzymes, molecular docking studies were performed using Maestro 11.1 (Schrödinger LLC).[44] X-ray crystal structures of hMAO-A (PDB IDs 2BXR and 2Z5X)[35,36] and AChE (PDB ID 1EVE)[37] enzymes were imported from the protein data bank (www.rscb.org). Protein was prepared using "protein preparation wizard" application of Schrödinger suite 2017. Energy was minimized using OPLS2005 force field. Ligands were drawn in ChemBio Draw Ultra-12 and prepared using ligand preparation application in Schrödinger suite 2017. For each compound, the top-score docking poses were chosen for final ligand-target interaction analysis employing XP interaction visualizer of Maestro 11.1 software. Validation of the docking procedure was done by redocking the cocrystallized ligand into the active site of the enzymes. The Qikprop application of Schrodinger suit was used to determine the drug like and ADME properties of the compounds.[45]

Molecular Dynamics Simulation Studies. In order to investigate the behavior and stability of the potent inhibitors into the active site of the MAO and AChE, molecular dynamic (MD) simulation was utilized. For this investigation, docking complexes of **VB1** with MAO-A and **VB8** with AChE were used. MD simulations were performed using the Desmond standard protocol.[46] Complex was solvated by TIP3P water model and then naturalized by adding 0.15 M Na^+ and Cl^- ions. The thickness of the water layer was set to 10 Å. Before

DOI: 10.1021/acschemneuro.8b00220
ACS Chem. Neurosci. 2019, 10, 252−265

the MD simulations, the systems were minimized with a maximum iteration of 2000 steps. Then, the systems were submitted to 30 ns MD simulation for equilibration and production MD run. Temperature and pressure were assigned on 300 K and 1.01325 bar, respectively, using the isothermal−isobaric (NPT) ensemble. A cutoff 9 Å was used for Coulomb interactions.

■ ASSOCIATED CONTENT

Supporting Information

The Supporting Information is available free of charge on the ACS Publications website at DOI: 10.1021/acschemneuro.8b00220.

NMR spectral data and HRMS graphs of the final compounds (PDF)

■ AUTHOR INFORMATION

Corresponding Author

*E-mails for V.K.: vinod.kumar@cup.edu.in; vpathania18@gmail.com. Tel.: +911642864214.

ORCID

Vinod Kumar: 0000-0002-1438-9438

Author Contributions

B.K. was involved in the design and synthesis of most of the compounds. He also performed hMAO and ee AChE inhibitory assays, performed *in silico* studies, and drafted the manuscript. A.R.D. was also involved in the synthesis of some of the compounds, column purification, and spectral analysis of the compounds. He also assisted in the molecular modeling studies and drafting of the manuscript. B.S. under the supervision of A.K.M., performed other *in vitro* biological studies like cytotoxic studies, ROS production inhibition potential, and neuroprotective studies. S.K.G. and S.K. conducted BuChE inhibition studies of the compounds. J.P. helped in the evaluation of hMAO and ee AChE inhibition activities and reversibility inhibition studies. V.K. conceptualized, supervised, and coordinated all the studies and prepared the final draft of the manuscript. All authors read and approved the final manuscript.

Notes

The authors declare the following competing financial interest(s): A patent application has been filed containing these compounds (Indian patent application number 201811008301).

■ ACKNOWLEDGMENTS

V.K. is thankful to the DST-SERB (EMR/2015/002339) and Central University of Punjab, Bathinda, (RSM GP25) for providing the financial assistance. B.K. is thankful to CUP, Bathinda and CSIR for the Senior Research Fellowship. J.P. is thankful to DST-SERB for the Research Grant (ECR/2015/000240).

■ ABBREVIATIONS

QPlogBB, qualitatively predicted logarithmic ratio between the concentration of a compound in brain and blood; LogP, partition coefficient of a molecule between an aqueous and lipophilic phase (octanol and water); CAS, Catalytic active site; PAS, Peripheral active site; MTT, 3-(4,5-dimethylthiazol-2-yl)-2,5-diphenyltetrazolium; 6-OHDA, 6-hydroxydopamine; DMEM, Dulbecco's Modified Eagle's medium; HEPES, (4-(2-hydroxyethyl)-1-piperazineethanesulfonic acid)

■ REFERENCES

(1) Goedert, M., and Spillantini, M. G. (2006) A century of Alzheimer's disease. *Science 314*, 777−781.

(2) Alzheimer's Association (2017) Alzheimer's disease facts and figures. *Alzheimer's Dementia 13*, 325−373.

(3) Kung, H. F. (2012) The β-amyloid hypothesis in Alzheimer's disease: seeing is believing. *ACS Med. Chem. Lett. 3*, 265−267.

(4) Garcia-Alloza, M., Gil-Bea, F., Diez-Ariza, M., Chen, C.-H., Francis, P. T., Lasheras, B., and Ramirez, M. (2005) Cholinergic−serotonergic imbalance contributes to cognitive and behavioral symptoms in Alzheimer's disease. *Neuropsychologia 43*, 442−449.

(5) Cummings, J. L., Ross, W., Absher, J., Gornbein, J., and Hadjiaghai, L. (1995) Depressive symptoms in Alzheimer disease: assessment and determinants. *Alzheimer Dis. Assoc. Disord. 9*, 87−93.

(6) Kumar, B., Gupta, V., and Kumar, V. (2016) A Perspective on Monoamine Oxidase Enzyme as Drug Target: Challenges and Opportunities. *Curr. Drug Targets 18*, 87−97.

(7) Sano, M., Ernesto, C., Thomas, R. G., Klauber, M. R., Schafer, K., Grundman, M., Woodbury, P., Growdon, J., Cotman, C. W., Pfeiffer, E., et al. (1997) A controlled trial of selegiline, alpha-tocopherol, or both as treatment for Alzheimer's disease. *N. Engl. J. Med. 336*, 1216−1222.

(8) Müller, T. J., Braun, R., and Ansorge, M. (2000) A Novel Three-Component One-Pot Pyrimidine Synthesis Based upon a Coupling−Isomerization Sequence. *Org. Lett. 2*, 1967−1970.

(9) Sugimoto, H., Yamanish, Y., Iimura, Y., and Kawakami, Y. (2000) Donepezil hydrochloride (E2020) and other acetylcholinesterase inhibitors. *Curr. Med. Chem. 7*, 303−339.

(10) Marco-Contelles, J., do Carmo Carreiras, M., Rodríguez, C., Villarroya, M., and Garcia, A. G. (2006) Synthesis and pharmacology of galantamine. *Chem. Rev. 106*, 116−133.

(11) Anand, P., and Singh, B. (2013) A review on cholinesterase inhibitors for Alzheimer's disease. *Arch. Pharmacal Res. 36*, 375−399.

(12) Racchi, M., Mazzucchelli, M., Porrello, E., Lanni, C., and Govoni, S. (2004) Acetylcholinesterase inhibitors: novel activities of old molecules. *Pharmacol. Res. 50*, 441−451.

(13) Gura, T. (2008) Hope in Alzheimer's fight emerges from unexpected places. *Nat. Med. 14*, 894−894.

(14) Munoz-Torrero, D. (2008) Acetylcholinesterase inhibitors as disease-modifying therapies for Alzheimer's disease. *Curr. Med. Chem. 15*, 2433−2455.

(15) Yiannopoulou, K. G., and Papageorgiou, S. G. (2013) Current and future treatments for Alzheimer's disease. *Ther. Adv. Neurol. Disord. 6*, 19−33.

(16) Small, G. W., and Greenfield, S. (2015) Current and future treatments for Alzheimer disease. *Am. J. Geriatric Psychiatry 23*, 1101−1105.

(17) Oset-Gasque, M. J. S., and Marco-Contelles, J. (2018) Alzheimer's Disease, the "One-Molecule, One-Target" Paradigm, and the Multitarget Directed Ligand Approach. *ACS Chem. Neurosci. 9*, 401−403.

(18) Oliveira Pedrosa, M. D., Duarte da Cruz, R., Oliveira Viana, J., de Moura, R. O., Ishiki, H. M., Barbosa Filho, F., Diniz, M. F., Scotti, M., Scotti, L., and Bezerra Mendonca, F. (2017) Hybrid Compounds as Direct Multitarget Ligands: A Review. *Curr. Top. Med. Chem. 17*, 1044−1079.

(19) Pisani, L., Farina, R., Soto-Otero, R., Denora, N., Mangiatordi, G. F., Nicolotti, O., Mendez-Alvarez, E., Altomare, C. D., Catto, M., and Carotti, A. (2016) Searching for multi-targeting neurotherapeutics against Alzheimer's: Discovery of potent AChE-MAO B inhibitors through the decoration of the 2H-chromen-2-one structural motif. *Molecules 21*, 362.

(20) Yanez, M., and Vina, D. (2013) Dual inhibitors of monoamine oxidase and cholinesterase for the treatment of Alzheimer disease. *Curr. Top. Med. Chem. 13*, 1692−1706.

DOI: 10.1021/acschemneuro.8b00220
ACS Chem. Neurosci. 2019, 10, 252−265

(21) Kumar, B., Sheetal, Mantha, A. K., and Kumar, V. (2016) Recent developments on the structure−activity relationship studies of MAO inhibitors and their role in different neurological disorders. *RSC Adv. 6*, 42660−42683.
(22) Agis-Torres, A., Sollhuber, M., Fernandez, M., and Sanchez-Montero, J. (2014) Multi-target-directed ligands and other therapeutic strategies in the search of a real solution for Alzheimer's disease. *Curr. Neuropharmacol. 12*, 2−36.
(23) Kumar, B., Sheetal, Mantha, A. K., and Kumar, V. (2018) Synthesis, Biological Evaluation and Molecular Modeling Studies of Phenyl-/Benzhydrylpiperazine Derivatives as Potential MAO Inhibitors. *Bioorg. Chem. 77*, 252−262.
(24) Kumar, B., Kumar, M., Dwivedi, A. R., and Kumar, V. (2018) Synthesis, Biological Evaluation and Molecular Modeling Studies of Propargyl-Containing 2, 4, 6-Trisubstituted Pyrimidine Derivatives as Potential Anti-Parkinson Agents. *ChemMedChem 13*, 705−712.
(25) Bolea, I., Juárez-Jiménez, J., de los Rıos, C. B., Chioua, M., Pouplana, R. N., Luque, F. J., Unzeta, M., Marco-Contelles, J., and Samadi, A. (2011) Synthesis, biological evaluation, and molecular modeling of donepezil and N-[(5-(benzyloxy)-1-methyl-1 H-indol-2-yl) methyl]-N-methylprop-2-yn-1-amine hybrids as new multipotent cholinesterase/monoamine oxidase inhibitors for the treatment of Alzheimer's disease. *J. Med. Chem. 54*, 8251−8270.
(26) Weinreb, O., Amit, T., Bar-Am, O., and Youdim, M. B. (2010) Rasagiline: a novel anti-Parkinsonian monoamine oxidase-B inhibitor with neuroprotective activity. *Prog. Neurobiol. 92*, 330−344.
(27) Hughes, R. E., Nikolic, K., and Ramsay, R. R. (2016) One for All? Hitting Multiple Alzheimer's Disease Targets with One Drug. *Front. Neurosci. 10*, Article No. 177.
(28) Samadi, A., Chioua, M., Bolea, I., de los Rios, C., Iriepa, I., Moraleda, I., Bastida, A., Esteban, G., Unzeta, M., Galvez, E., and Marco-Contelles, J. (2011) Synthesis, biological assessment and molecular modeling of new multipotent MAO and cholinesterase inhibitors as potential drugs for the treatment of Alzheimer's disease. *Eur. J. Med. Chem. 46*, 4665−4668.
(29) Chimenti, F., Carradori, S., Secci, D., Bolasco, A., Bizzarri, B., Chimenti, P., Granese, A., Yanez, M., and Orallo, F. (2010) Synthesis and inhibitory activity against human monoamine oxidase of N1-thiocarbamoyl-3, 5-di (hetero) aryl-4, 5-dihydro-(1H)-pyrazole derivatives. *Eur. J. Med. Chem. 45*, 800−804.
(30) Mostert, S., Mentz, W., Petzer, A., Bergh, J. J., and Petzer, J. P. (2012) Inhibition of monoamine oxidase by 8-[(phenylethyl) sulfanyl] caffeine analogues. *Bioorg. Med. Chem. 20*, 7040−7050.
(31) Minders, C., Petzer, J. P., Petzer, A., and Lourens, A. C. (2015) Monoamine oxidase inhibitory activities of heterocyclic chalcones. *Bioorg. Med. Chem. Lett. 25*, 5270−5276.
(32) Pizzinat, N., Copin, N., Vindis, C., Parini, A., and Cambon, C. (1999) Reactive oxygen species production by monoamine oxidases in intact cells. *Naunyn-Schmiedeberg's Arch. Pharmacol. 359*, 428−431.
(33) Sturza, A., Noveanu, L., Duicu, O., Angoulvant, D., and Muntean, D. M. (2014) 0209: Monoamine oxidases as novel sources of reactive oxygen species in experimental diabetes. *Arch. Cardiovasc. Dis. 6*, 15.
(34) Xie, H.-R., Hu, L.-S., and Li, G.-Y. (2010) SH-SY5Y human neuroblastoma cell line: in vitro cell model of dopaminergic neurons in Parkinson's disease. *J. Vis. Exp. 123*, 1086−1092.
(35) De Colibus, L., Li, M., Binda, C., Lustig, A., Edmondson, D. E., and Mattevi, A. (2005) Three-dimensional structure of human monoamine oxidase A (MAO A): relation to the structures of rat MAO A and human MAO B. *Proc. Natl. Acad. Sci. U. S. A. 102*, 12684−12689.
(36) Son, S.-Y., Ma, J., Kondou, Y., Yoshimura, M., Yamashita, E., and Tsukihara, T. (2008) Structure of human monoamine oxidase A at 2.2-Å resolution: the control of opening the entry for substrates/inhibitors. *Proc. Natl. Acad. Sci. U. S. A. 105*, 5739−5744.
(37) Cheung, J., Rudolph, M. J., Burshteyn, F., Cassidy, M. S., Gary, E. N., Love, J., Franklin, M. C., and Height, J. J. (2012) Structures of human acetylcholinesterase in complex with pharmacologically important ligands. *J. Med. Chem. 55*, 10282−10286.
(38) Kalb, A., von Haefen, C., Sifringer, M., Tegethoff, A., Paeschke, N., Kostova, M., Feldheiser, A., and Spies, C. D. (2013) Acetylcholinesterase inhibitors reduce neuroinflammation and-degeneration in the cortex and hippocampus of a surgery stress rat model. *PLoS One 8*, e62679.
(39) Kumar, D., Gupta, S. K., Ganeshpurkar, A., Gutti, G., Krishnamurthy, S., Modi, G., and Singh, S. K. (2018) Development of Piperazinediones as dual inhibitor for treatment of Alzheimer's disease. *Eur. J. Med. Chem. 150*, 87−101.
(40) Kaur, N., Dhiman, M., Perez-Polo, J. R., and Mantha, A. K. (2015) Ginkgolide B revamps neuroprotective role of apurinic/apyrimidinic endonuclease 1 and mitochondrial oxidative phosphorylation against Aβ25−35-induced neurotoxicity in human neuroblastoma cells. *J. Neurosci. Res. 93*, 938−947.
(41) Liang, Z., Shi, F., Wang, Y., Lu, L., Zhang, Z., Wang, X., and Wang, X. (2011) Neuroprotective effects of tenuigenin in a SH-SY5Y cell model with 6-OHDA-induced injury. *Neurosci. Lett. 497*, 104−109.
(42) Cai, P., Fang, S.-Q., Yang, X.-L., Wu, J.-J., Liu, Q.-H., Hong, H., Wang, X.-B., and Kong, L.-Y. (2017) Rational Design and Multibiological Profiling of Novel Donepezil−Trolox Hybrids against Alzheimer's Disease, with Cholinergic, Antioxidant, Neuroprotective, and Cognition Enhancing Properties. *ACS Chem. Neurosci. 8*, 2496−2511.
(43) Yan, J., Hu, J., Liu, A., He, L., Li, X., and Wei, H. (2017) Design, synthesis, and evaluation of multitarget-directed ligands against Alzheimer's disease based on the fusion of donepezil and curcumin. *Bioorg. Med. Chem. 25*, 2946−2955.
(44) Friesner, R. A., Murphy, R. B., Repasky, M. P., Frye, L. L., Greenwood, J. R., Halgren, T. A., Sanschagrin, P. C., and Mainz, D. T. (2006) Extra precision glide: Docking and scoring incorporating a model of hydrophobic enclosure for protein− ligand complexes. *J. Med. Chem. 49*, 6177−6196.
(45) Release, Q. S. (2017) *QikProp*, Schrödinger, LLC, New York, NY.
(46) Release, S. (2014) *Desmond Molecular Dynamics System, version 3.7* and *Maestro−Desmond Interoperability Tools, version 3*, DE Shaw Research, New York, NY.

DOI: 10.1021/acschemneuro.8b00220
ACS Chem. Neurosci. 2019, 10, 252−265